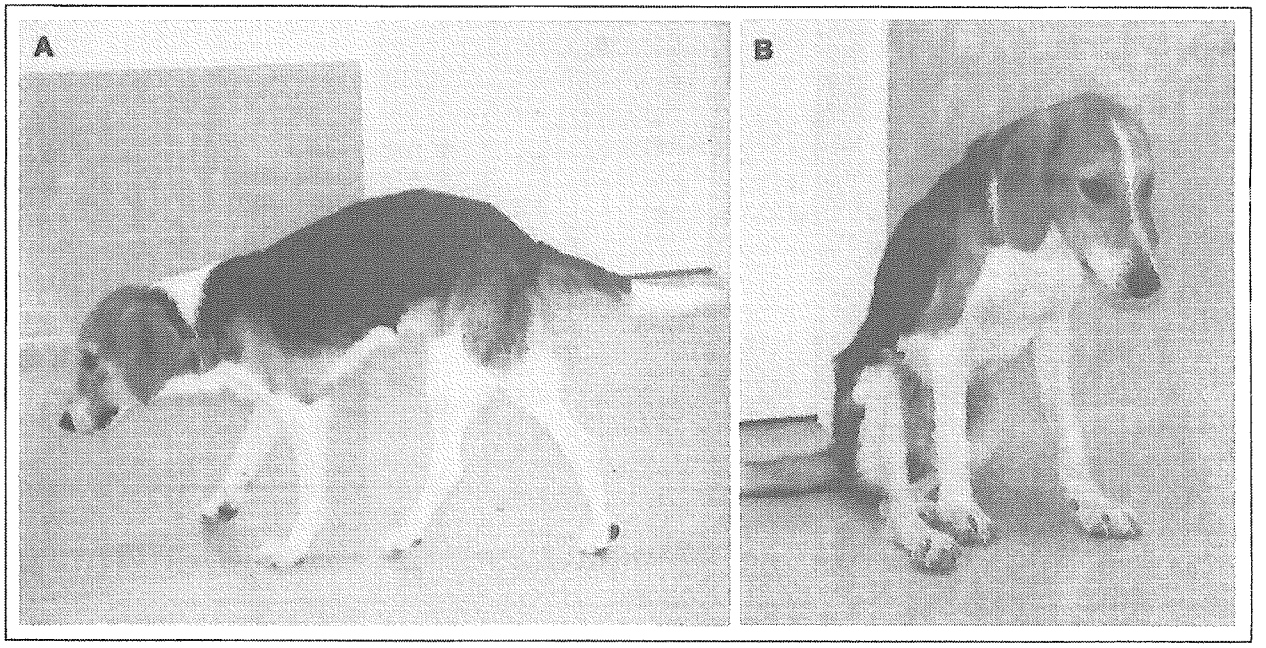

Figure 3. A representative affected G3 male dog at 12 months of age.
(**A**) When walking, spine curvature, supinate front paws, and drop feet in hind limbs were observed.
(**B**) Severe temporal muscle atrophy and throwing of hind limbs when sitting were recognized.

showed gait and mobility disturbances, and progressive tongue enlargement, dysphagia, feeding difficulty, and excessive salivation were also recognized [15]. We, therefore, evaluated the clinical phenotypes of affected G3 male dogs at the ages of 1, 2, 4, 6, and 12 months.

Within a week after the birth, affected pups were slightly less active than normal littermates during the period. Around 2 months of age, dystrophic pups sometimes sit with hind legs extended. The dog showed stiff limbs, but these symptoms were probably related to contraction of the joints. Soon after, they move the hind limbs simultaneously (bunny-hops with hind legs) (**Fig. 4A and B**). Distal limb muscle atrophy appeared from 2 months of age in the dogs (**Fig. 4C**), but proximal limb muscle atrophy in G3 males was observed at 4 months of age (**Fig. 4D**). Proximal limb muscle, especially thigh muscle, has been spared at the relatively early period, but that was severer than distal limb muscle atrophy at 12 months of age (**Fig. 3A**). The temporal muscle was also involved at the age of 2 months, and it was much more atrophied than other muscles at the age of 12 months (**Fig. 3B and 4E**). Around 4 months of age, they occasionally dribbled saliva when sitting. They frequently showed tongue hypertrophy (**Fig. 4F and G**), and inability to open the jaw due to contracture of the joints. 40% of dogs showed difficulty in eating food or swallowing at the age of 6 months (**Fig. 4H**), therefore hand feeding is sometimes required for the dogs. An enlarged and thickened tongue was seen in all affected G3 males at 12 months of age. To ascertain the degree of jaw joint contracture, we examined the maximum mouth opening in both normal and affected G3 males (**Fig. 4I**). The extent of the opening in normal G3 males increased with age, but it did not change much in the affected G3 dogs. The difference between them was significant at 4, 6, and 12 months of age, therefore jaw joint contracture probably started around 4 months of age in G3 affected dogs.

Macroscopic and histopathological findings

The diaphragm muscle of a normal G3 male that died at 1 day of age did not show streaks in the muscular portions (**Fig. 5A**); however, there were many radiating white streaks in an affected G3 male that died at 1 day of age (data not shown) as well as in another affected G3 male that was sacrificed at 3 days of age (**Fig. 5D**). Histopathological examination of the diaphragm muscle in a sacrificed, affected G3 male at 3 days of age showed acute stage of diffuse muscle necrosis with edema (**Fig. 5E**). At the age of 6 months, the

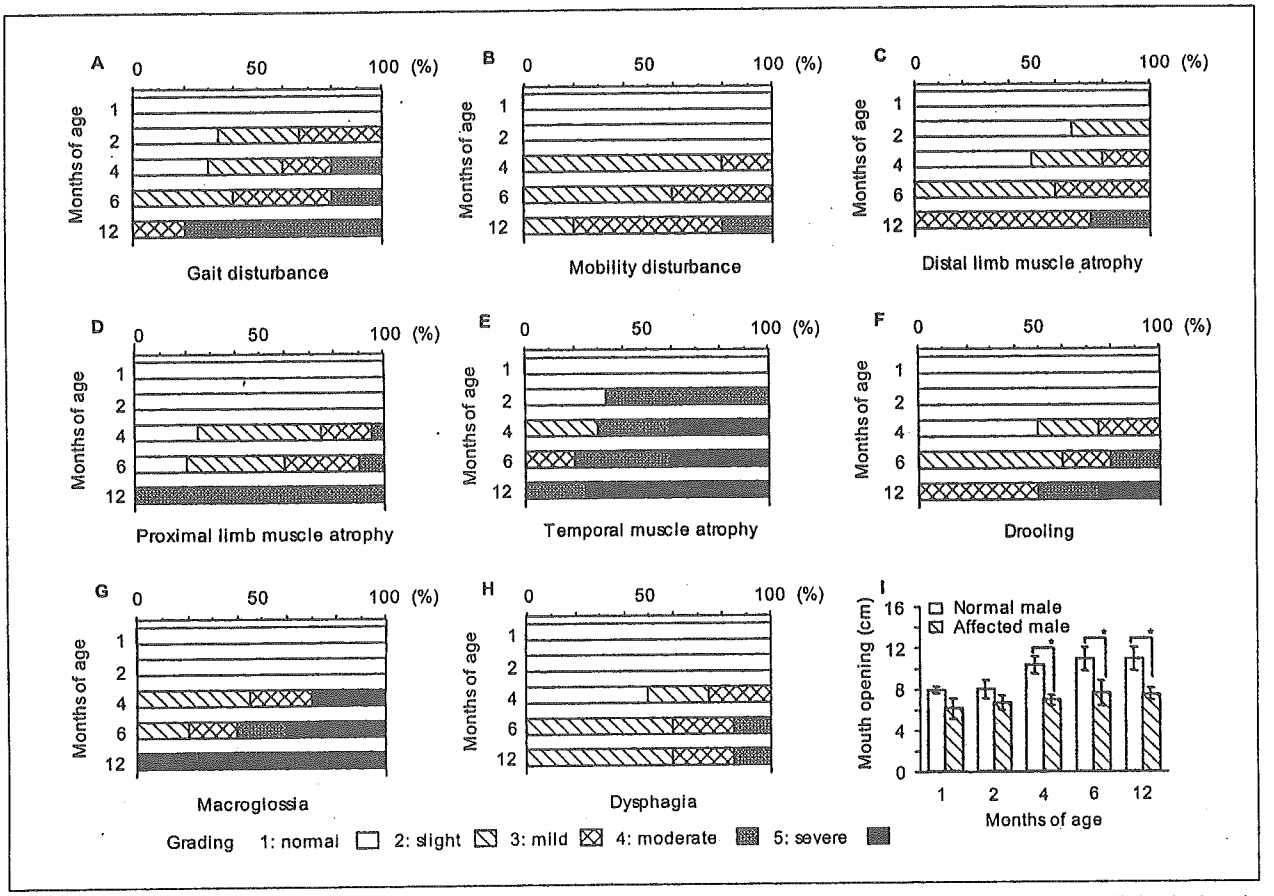

Figure 4. Evaluation of clinical phenotypes in affected G3 male dogs. The evaluation of each clinical sign is shown in **A-H**: (**A**) gait disturbance, (**B**) mobility disturbance (**C**) distal limb, (**D**) proximal limb, (**E**) and temporal muscle atrophy, (**F**) drooling, (**G**) macroglossia, and (**H**) dysphagia at the ages of 1, 2, 4, 6, and 12 months. The severity of each sign in affected G3 dogs was classified into five grades as described in Materials and Methods and Table. The percentage of affected G3 dogs in each grade was calculated for each month of age. (**I**) Maximum mouth opening in normal and affected G3 male dogs at the ages of 1, 2, 4, 6, and 12 months. Bar: mean ± S.E.; $*p < 0.05$.

diaphragma muscle in an affected G3 male disclosed marked variation in fiber size and increase in fibrosis and necrotic fibers (**Fig. 5F**).

The diameter of the fibers in the anterior tibial muscle increased with age in normal G3 males (**Fig. 6A-C**), while the muscle in the sacrificed, affected G3 male at 3 days of age showed slight fiber size variation and some necrotic fibers (**Fig. 6D**). The findings were not different from those in an affected G3 male that died at 1 day of age (data not shown). At the age of 2 months, the tibial muscle from an affected G3 male displayed an increase in the number of necrotic fibers, invasion of inflammatory cells, and a slight proliferation of the interstitial tissues (**Fig. 6E**). At the age of 6 months, marked fiber size variation, increase in the interstitial fibrosis, and hypertrophied or centrally nucleated fibers were observed (**Fig. 6F**).

In macroscopic examinations, an affected G3 male at the age of 12 months had severe hypertrophy of the tongue, genioglossus, and geniohyoideus muscles (**Fig. 7B**) as compared with those in a normal male (**Fig. 7A**). In the tongue muscle, there were many hypertrophied fibers and opaque fibers (**Fig. 7D**), as compared with those in the normal male (**Fig. 7C**).

Discussion

In this report, we described the major clinical and histopathological phenotypes of beagle-based dystrophic dogs, $CXMD_J$, that carried the same *dystrophin* gene mutation as CXMD dogs. We

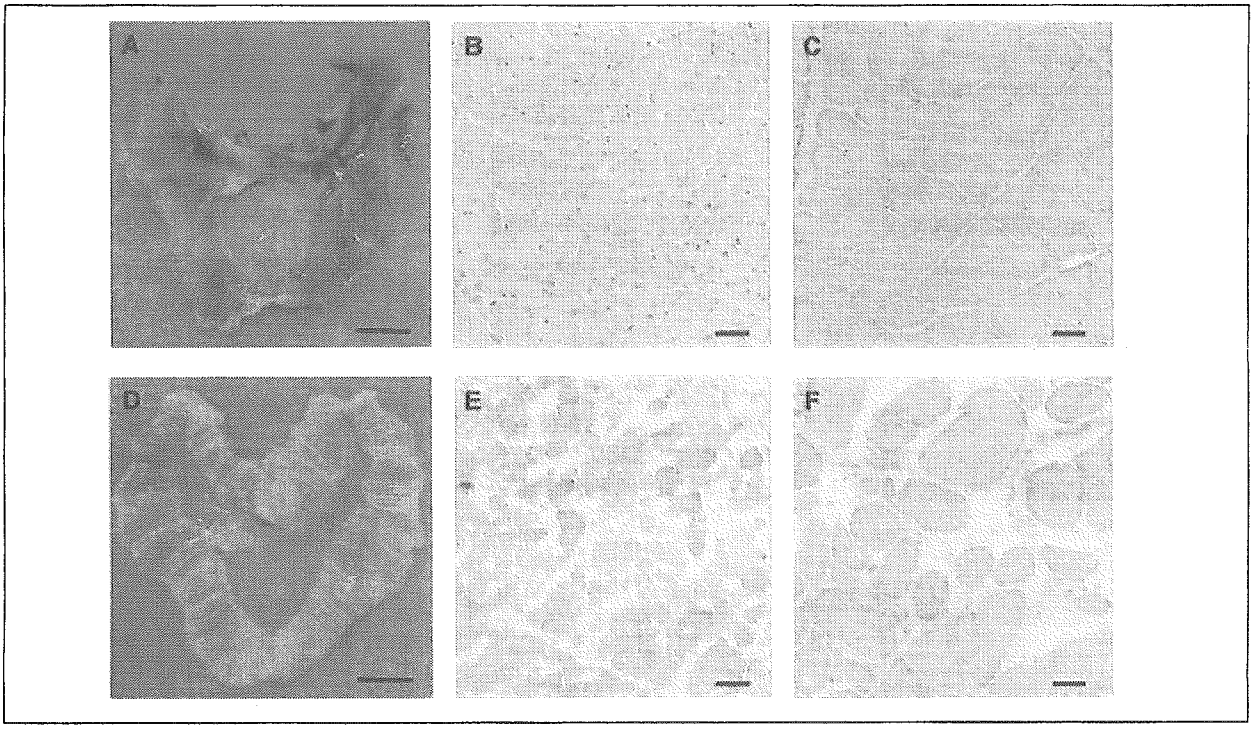

Figure 5. Macroscopy and histopathology of diaphragm muscles. Diaphragm of a normal G3 male dog that died at 1 day of age (**A**) and an affected G3 male dog that was sacrificed at 3 days of age (**D**). Bar = 1 cm. H&E staining of cross-sections of diaphragm muscles from normal G3 male at 3 day of age (**B**) and at 6 months of age (**C**), and from affected G3 males that was sacrificed at 3 days of age (**E**) and 6 months of age (**F**). Bar = 50 μm.

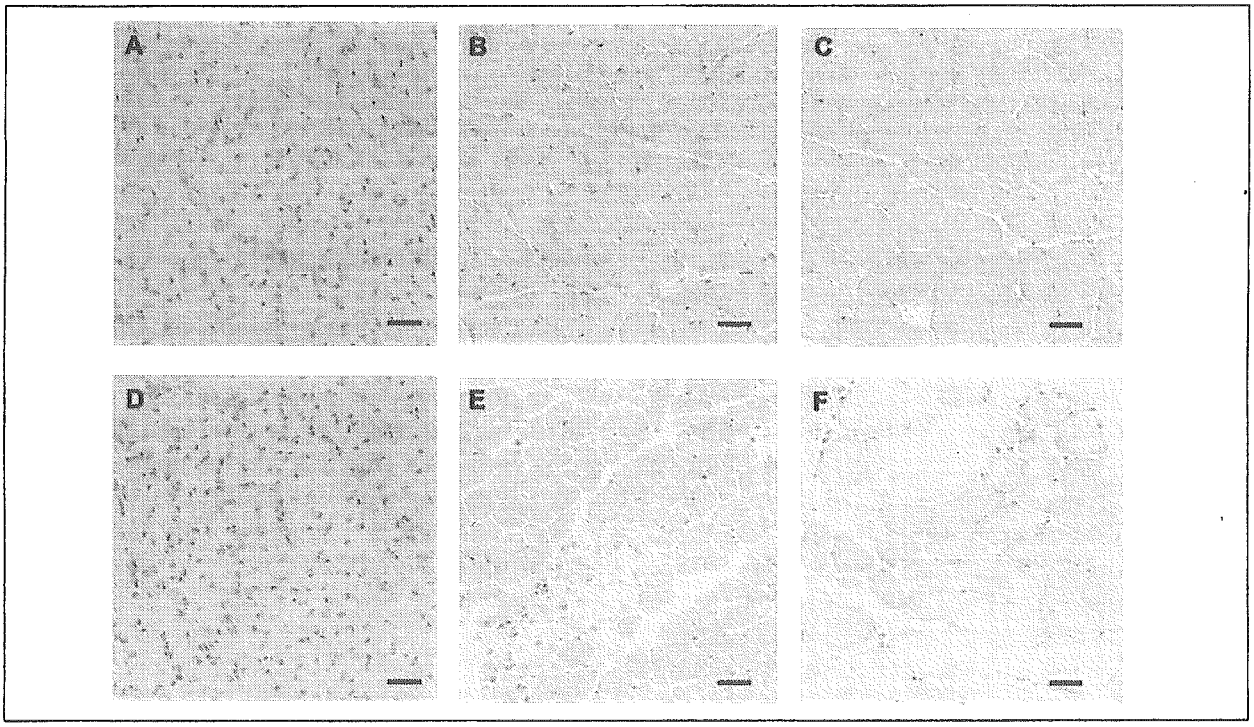

Figure 6. Histopathology of anterior tibial muscles. H&E staining of cross-sections of anterior tibial muscles from normal G3 male at 3 days of age (**A**), 2 month of age (**B**), and 6 months of age (**C**), and from affected G3 male at 3 days of age (**D**), 2 month of age (**E**), and 6 months of age (**F**). Bar = 50 μm.

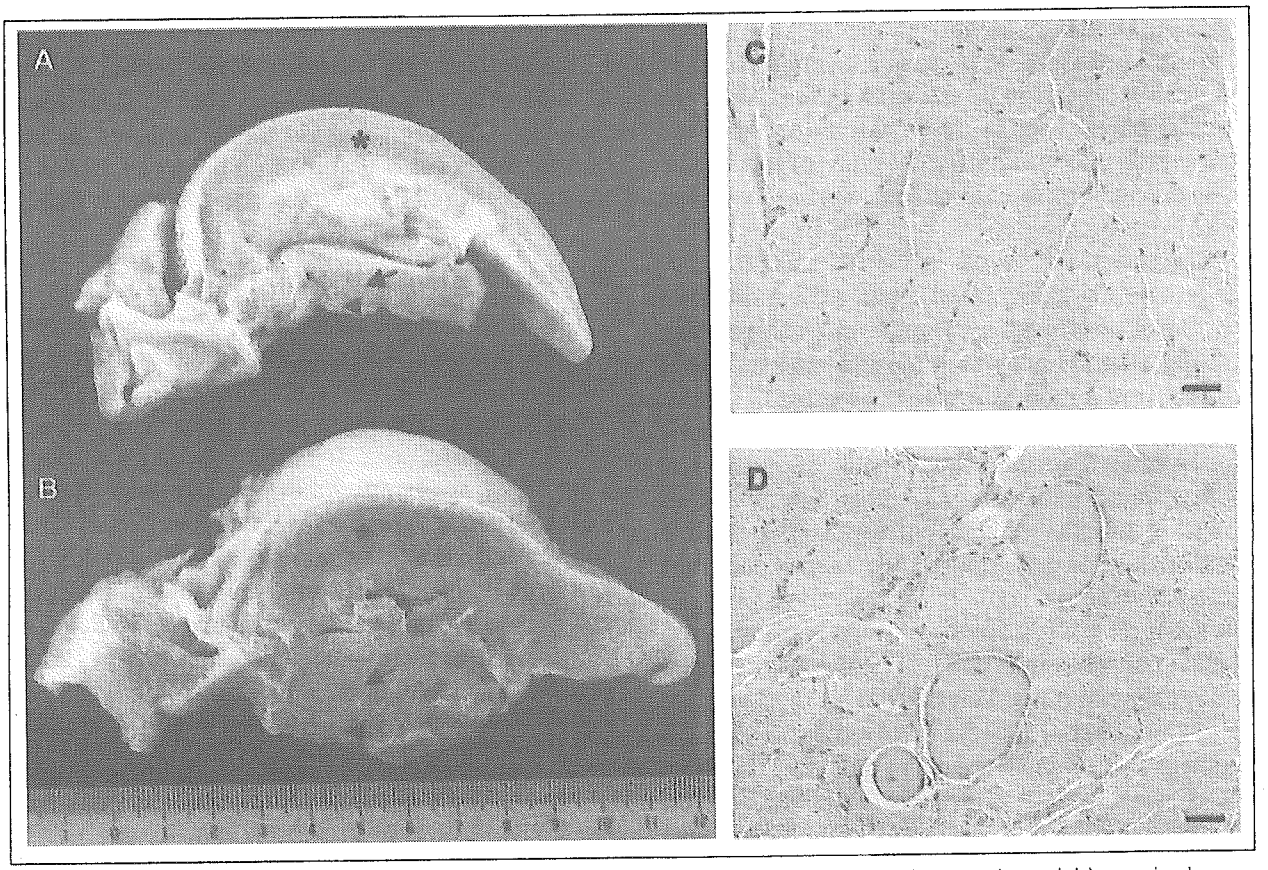

Figure 7. Macroscopy and histopathology of tongue and sublingual muscles. Tongue (asterisk), genioglossus (arrow) and geniohyoideus (arrowhead) muscles in a normal G3 male (**A**) and an affected G3 male (**B**) at 12 months of age. Bar = 1 cm. H&E staining of cross-sections of the tongue muscle from a normal G3 male (**C**) and an affected G3 male (**D**) at 12 months of age. Bar = 50 μm.

dealt mainly with the third generation of dystrophic dogs, G3, when they still have mixture of both beagle and golden retriever backgrounds. However, the size of G3 CXMD$_J$ was smaller and easier to handle than golden retriever-based CXMD dogs [16].

The serum CK levels in affected G3 dogs reached two peaks during the course: the first peak occurred immediately after birth and the second peak at two months after birth. This particular pattern of serum CK levels was also seen in G3 carrier females, although the increase was quite small. Previous researchers have reported that serum CK levels in CXMD dogs were much higher than those in normal littermates shortly after birth [15, 17] and had another peak at 6 to 8 weeks after birth [15]. The profiles of serum CK levels in our dystrophic G3 dogs corresponded well with these reports.

The elevation of serum CK levels in G3 affected and carrier female dogs shortly after birth may be a result of acute generalized muscle damage after the stress of whelping. It is very important to note that 32.3% of affected G3 male pups had died by 3 days of age, and the rate was significantly higher than that of normal dogs. Actually, it has been reported that 28.0% or 45.5% CXMD pups died with a neonatal fulminant form within the first 2 weeks after birth [15, 18]. Although the cause has not been fully elucidated, acute respiratory failure might be associated with the pathogenesis of the early death because involvement of the diaphragm muscle was seen in neonatal fulminant CXMD pups [19] as well as in affected G3 dogs at three days after birth (**Fig. 5E**). The stress of whelping is one factor that may exacerbate involvement of the diaphragm. Moreover, Nguyen et al. reported selective involvement of the diaphragm muscle in neonatal CXMD pups, and they found that anterior tibial muscle damage was not more severe than that of the diaphragm muscle [19]. In affected G3 dogs, a similar selec-

tive pattern was observed at the neonatal stage (**Fig. 5E and 6D**). It is very intriguing to note that genetic variation of sire may influence on the neonatal phenotypes of dystrophic dogs, since the same carrier produced different types of dystrophic pups: neonatal fulminant or less severe dystrophic pups.

The serum CK levels in G3 affected and carrier female dogs increased again at 2 months of age. Onset of clinical symptoms, such as gait and mobility disturbances and muscle atrophy, were definite from 2 months of age in affected G3 males (**Fig. 4A-E**). The onset of the disease might be closely related to the second peak of serum CK that we found in affected G3 dogs. The period of around 2 months of age corresponds to canine socialization for developing spontaneous activities after the weaning [20]. It is, therefore, possible that the increase in activity of pups may effect on an elevation of serum CK levels and on the onset of clinical symptoms. Valentine et al. reported that the age of onset of muscle involvement in CXMD dogs was from 8 to 10 weeks of age [4, 15]. Those results were largely consistent with the data on our affected G3 dogs. On the other hand, they also reported that the disease severity in affected beagle-crossed dogs was milder than that in CXMD dogs around the age of 8 weeks [15]. The same criteria could be required to evaluate and compare affected G3 dogs with CXMD dogs.

The feeding difficulty and jaw joint contracture were apparent from 4 months of age (**Fig. 4F-I**). At 6 months of age, histopathological findings of diaphragm (**Fig. 5F**) and anterior tibial (**Fig. 6F**) muscles in affected G3 male dogs were compatible with those in CXMD dogs at 6 months of age [21]. All affected G3 dogs at the age of 12 months showed severe macroglossia and hypertrophy of the sublingual muscles (**Fig. 7B**). Degeneration of tongue muscle fibers has been noted as early as the neonatal stage in CXMD [18, 19], although we have not confirmed that. Elucidation of tongue and sublingual muscle involvement in dystrophic dogs is indispensable, because dysphagia is now one of the major symptoms in older DMD patients [22, 23].

Finally, we here showed the characteristics of G3 CXMD$_J$, and especially emphasized the particular change of serum CK levels with age, not only in G3 CXMD$_J$ but also in female carrier dogs. The extremely high CK values we found in neonatal dystrophic dogs may reflect respiratory muscle damage due to stress during whelping. These findings in G3 CXMD$_J$ dogs were similar to those in CXMD dogs; therefore, CXMD$_J$ is a useful model for investigation of the pathogenesis of and development of therapies for dystrophin-deficient muscular dystrophy, DMD.

Acknowledgements

We thank Naoko Yugeta, D.V.M. (School of Veterinary Medicine, Azabu University) for advising on the healthy care of dogs and also thank Hideki Kita, Shinichi Ichikawa, Yumiko Yahata, and Kazue Kinoshita (JAC, Inc., Tokyo) for keeping of dogs. This study was supported by Grants-in-Aid for Research on Nervous and Mental Disorders (13B-1, 16B-2) and Health Sciences Research Grants for Research on Psychiatric and Neurological Diseases and Mental Health (H12-kokoro-025, H15-kokoro-021), the Human Genome and Gene Therapy (H13-genome-001, H16-genome-003) from the Ministry of Health, Labor and Welfare of Japan, and Grants-in-Aid for Scientific Research from the Ministry of Education, Science, Sports and Culture of Japan (to Y.S. and S.T.).

References

1. Moser H. Duchenne muscular dystrophy: pathogenetic aspects and genetic prevention. Hum Genet 1984;66:17-40.
2. Koenig M, Hoffman EP, Bertelson CJ, et al. Complete cloning of the Duchenne muscular dystrophy (DMD) cDNA and preliminary genomic organization of the DMD gene in normal and affected individuals. Cell 1987;50:509-17.
3. Bulfield G, Siller WG, Wight PA, et al. X chromosome-linked muscular dystrophy (*mdx*) in the mouse. Proc Natl Acad Sci USA 1984;81:1189-92.
4. Valentine BA, Cooper BJ, Cummings JF, et al. Progressive muscular dystrophy in a golden retriever dog: light microscope and ultrastructural features at 4 and 8 months. Acta Neuropathol (Berl) 1986;71:301-10.
5. Cooper BJ, Winand NJ, Stedman H, et al. The homologue of the Duchenne locus is defective in X-linked muscular dystrophy of dogs. Nature 1988;334:154-6.
6. Kornegay JN, Tuler SM, Miller DM, et al. Muscular dystrophy in a litter of golden retriever dogs. Muscle Nerve 1988;11:1056-64.
7. Valentine BA, Winand NJ, Pradhan D, et al. Canine X-linked muscular dystrophy as an animal model of Duchenne muscular dystrophy: a review. Am J Med Genet 1992;42:352-6.
8. Shelton GD, Engvall E. Canine and feline models of human inherited muscle diseases. Neuromuscul Disord 2005; 15:127-38.
9. Shimatsu Y, Katagiri K, Furuta T, et al. Canine X-linked muscular dystrophy in Japan (CXMD$_J$). Exp Anim 2003;52:93-7.

10. Yasuda S, Townsend D, Michele DE, et al. Dystrophic heart failure blocked by membrane sealant poloxamer. Nature 2005;436:1025-9.
11. Yoshimura M, Sakamoto M, Ikemoto M, et al. AAV vector-mediated microdystrophin expression in a relatively small percentage of mdx myofibers improved the mdx phenotype. Mol Ther 2004;10:821-8.
12. Dezawa M, Ishikawa H, Itokazu Y, et al. Bone marrow stromal cells generate muscle cells and repair muscle degeneration. Science 2005;309:314-7.
13. Dell'Agnola C, Wang Z, Storb R, et al. Hematopoietic stem cell transplantation does not restore dystrophin expression in Duchenne muscular dystrophy dogs. Blood 2004;104:4311-8.
14. Wilton SD, Honeyman K, Fletcher S, et al. Snapback SSCP analysis: engineered conformation changes for the rapid typing of known mutations. Hum Mutat 1998;11:252-8.
15. Valentine BA, Cooper BJ, de Lahunta A, et al. Canine X-linked muscular dystrophy. An animal model of Duchenne muscular dystrophy: clinical studies. J Neurol Sci 1988;88:69-81.
16. Kornegay JN, Bogan DJ, Bogan JR, et al. Contraction force generated by tarsal joint flexion and extension in dogs with golden retriever muscular dystrophy. J Neurol Sci 1999;166:115-21.
17. Bartlett RJ, Winand NJ, Secore SL, et al. Mutation segregation and rapid carrier detection of X-linked muscular dystrophy in dogs. Am J Vet Res 1996;57:650-4.
18. Valentine BA, Cooper BJ. Canine X-linked muscular dystrophy: selective involvement of muscles in neonatal dogs. Neuromuscul Disord 1991;1:31-8.
19. Nguyen F, Cherel Y, Guigand L, et al. Muscle lesions associated with dystrophin deficiency in neonatal golden retriever puppies. J Comp Pathol 2002;126:100-8.
20. Seksel K. Puppy socialization classes. Vet Clin North Am Small Anim Pract 1997;27:465-77.
21. Valentine BA, Cooper BJ, Cummings JF, et al. Canine X-linked muscular dystrophy: morphologic lesions. J Neurol Sci 1990;97:1-23.
22. Jaffe KM, McDonald CM, Ingman E, et al. Symptoms of upper gastrointestinal dysfunction in Duchenne muscular dystrophy: case-control study. Arch Phys Med Rehabil 1990;71:742-4.
23. Willig TN, Paulus J, Lacau Saint Guily J, et al. Swallowing problems in neuromuscular disorders. Arch Phys Med Rehabil 1994;75:1175-81.

American Journal of Pathology, Vol. 166, No. 6, June 2005

Musculoskeletal Pathology

Participation of Bone Marrow-Derived Cells in Fibrotic Changes in Denervated Skeletal Muscle

Yasushi Mochizuki,*† Koichi Ojima,* Akiyoshi Uezumi,* Satoru Masuda,* Kotaro Yoshimura,† and Shin'ichi Takeda*

From the Department of Molecular Therapy, National Institute of Neuroscience, National Center of Neurology and Psychiatry, Ogawa-higashi-cho, Kodaira, Tokyo; and the Department of Plastic and Reconstructive Surgery,† Graduate School of Medicine, The University of Tokyo, Hongo, Bunkyo-ku, Tokyo, Japan*

In denervated skeletal muscle, mononuclear interstitial cells accumulate in the perisynaptic regions before fibrotic change occurs. These cells are currently considered to be fibroblasts that originate from muscle tissue. However, when we denervated hind limbs of GFP-bone marrow chimeric mice by excising the sciatic nerve unilaterally, many bone marrow-derived cells (BM-DCs) infiltrated the interstitial spaces and accumulated in the perisynaptic regions, peaking 14 days after denervation. They accounted for nearly one-half of the increase in mononuclear interstitial cells. Although BM-DCs did not incorporate into satellite cells, immunohistochemical and FACS analyses revealed that BM-DCs were both CD45 and CD11b positive, indicating that they were of macrophage/monocyte lineage. BrdU staining showed inactive proliferation of BM-DCs. Reverse transcriptase-polymerase chain reaction of mononuclear cells isolated by FACS revealed that BM-DCs did not express type I collagen or tenascin-C; however, they did express transforming growth factor-β1, suggesting that they regulate the fibrotic process. In contrast, muscle tissue-derived interstitial cells expressed type I collagen and tenascin-C, suggesting that these populations were the final effectors of fibrosis. These findings identify elementary targets that may regulate the migration, homing, differentiation, and function of BM-DCs, leading to amelioration of the excessive fibrosis of denervated skeletal muscle. *(Am J Pathol 2005, 166:1721–1732)*

Fibrotic change is often observed after subacute or chronic inflammation, and severe fibrosis of a vital organ such as the lung, liver, or kidney is sometimes fatal. Denervated skeletal muscle tissue also exhibits persistent fibrotic change, which is accompanied by muscle fiber atrophy. This fibrosis may obstruct the recovery of atrophied muscle fibers even after reinnervation.

The number of mononuclear interstitial cells increases before fibrotic change in denervated skeletal muscle,[1,2] but labeling peripheral blood cells with radioisotopes demonstrated that the increased interstitial cells were not derived from the circulatory system.[3] These additional interstitial cells have been identified morphologically by electron microscopy as fibroblasts because they have much rough endoplasmic reticulum in their cytoplasm, actin filaments in their processes, and collagen fibers around them.[4]

With the accumulation of interstitial cells in the perisynaptic regions, increased expression of several ECMs such as tenascin-C, fibronectin, neural cell adhesion molecule (N-CAM), and heparan sulfate proteoglycans are observed in denervated skeletal muscle.[5] According to an *in vitro* study, the accumulating interstitial cells are thought to have produced these ECMs.[6] Despite all of these findings, however, whether these interstitial cells are homogeneous or heterogeneous, their definition or identification by cell surface antigens and their roles *in vivo* are still unknown.

Recently, the incorporation of bone marrow-derived cells (BM-DCs), including mesenchymal stem cells[7] or side population cells,[8] into regenerating muscle[9] or dystrophic skeletal muscle[10] was noted. Transplantation of bone marrow cells from GFP transgenic mice allowed the identification of BM-DCs in the recipient mice. Participa-

Supported by the Center of Excellence, Research on Nervous and Mental Disorders (grants-in-aid 10B-1 and 13B-1), the Ministry of Health, Labor, and Welfare of Japan, Research on the Human Genome and Gene Therapy (Health Sciences research grants H10-genome-015 and H13-genome-001), a grant-in-aid for Scientific Research (B) from the Ministry of Education, Science, Sports, and Culture of Japan, and a Research Fellowship from the Japan Society for the Promotion of Science (to K.O.).

Accepted for publication February 15, 2005.

Address reprint requests to Shin'ichi Takeda, MD, PhD, Department of Molecular Therapy, National Institute of Neuroscience, National Center of Neurology and Psychiatry, 4-1-1 Ogawa-higashi-cho, Kodaira, Tokyo 187-8502, Japan. E-mail: takeda@ncnp.go.jp.

tion of BM-DCs was reported not only in the regeneration process, but also in atherosclerotic or fibrotic lesions.[11–13] These findings suggest that regulating migration, homing, proliferation, or differentiation of BM-DCs might lead to mitigation or prevention of these lesions.

To examine whether BM-DCs are also incorporated into pathological processes in skeletal muscle, we studied the origin of the increased interstitial cells in denervated skeletal muscle by using a bone marrow chimeric animal. Here, using GFP bone marrow chimeric mice, we show for the first time that a considerable proportion of these interstitial cells are bone marrow-derived, ie, they are not of traditional fibroblast lineage but of macrophage/monocyte lineage, and that they are a possible regulator of the muscle tissue-derived interstitial cells that might finally constitute the fibrosis.

Materials and Methods

Animals

C57BL/6J mice (B6 mice) and BALB/c mice were purchased from Nihon CLEA (Tokyo, Japan). C57BL/6J-*GFP*-transgenic mice[14] were kindly provided by Dr. Okabe (Osaka University, Japan). All procedures used on experimental animals were approved by the Experimental Animal Care and Use Committee at the National Institute of Neuroscience.

BM Chimeric Mice and Denervation

Whole bone marrow cells were collected from humeri, femurs, and tibias of 7- to 8-week-old donor GFP-transgenic mice by aspiration and flushing. Mononuclear cells were refined through 40-μm and subsequently 10-μm filters and next by centrifugation with Lympholite-M (Cedarlane, Hornby, Ontario, Canada), and then they were diluted to concentrations of 5 to 10 $\times$ 10^6 cells in 100 μl of phosphate-buffered saline (PBS). Female C57BL/6J mice (7- to 8-week old) were lethally irradiated with 9 Gy (Hitachi Medical Co., Tokyo, Japan) immediately before retro-orbital injection of the donor BM cells under general anesthesia with 0.05 mg/g (body weight) of pentobarbiturate (Nembutal). These mice were given drinking water containing 1 mg/ml of ampicillin for 2 weeks after the transplantation.

Twelve weeks after the transplantation, the left sciatic nerve of the bone marrow recipients was excised for nearly the full length of the thigh (approximately 10 mm) from a small incision (approximately 4 mm) made in the mid-lateral thigh under general anesthesia and a surgical microscope (Olympus, Tokyo, Japan). The mice were sacrificed 1 day (day 1) to 4 months (day 112) after denervation by cervical dislocation under general anesthesia. The left gastrocnemius muscle was excised for analysis. The right gastrocnemius muscle served as the control sample. Bone marrow cells simultaneously collected from the femur were purified and then were analyzed by FACS (FACS VantageSE flow cytometer; Falcon, Franklin Lakes, NJ) to determine the bone marrow chimerism as a percentage of GFP-positive cells.

Immunohistochemistry

Muscle samples were fixed with 4% formaldehyde in PBS for 30 minutes and washed with 10% sucrose in PBS for 6 hours and then with 20% sucrose overnight. The samples were then soaked in OCT compound and frozen in isopentane cooled in liquid nitrogen. Serial cryostat sections (10 μm thick) were stained with hematoxylin and eosin (H&E) or immunohistochemically as described below. Sections were washed with PBS for 30 minutes, blocked with 1% bovine serum albumin, and then were reacted with first (37°C, 1 hour) and second (room temperature, 30 minutes) antibodies. Nuclei were stained with TOTO-3 (room temperature, 10 minutes). After staining, the sections were examined under a confocal laser-scanning microscope (Leica TCS SP; Leica, Heidelberg, Germany). To count GFP-positive cells, five randomly selected high-power fields of neuromuscular junction-rich and -poor areas were examined.

Western Blotting Analysis

Twenty to 40 cryostat sections of day 28 or day 112 gastrocnemius muscles were dissolved with 4 volumes (w/v) of sample buffer (10% SDS, 70 mmol/L Tris-HCl (pH 6.7), 10 mmol/L EDTA, and 5% β-mercaptoethanol), boiled for 5 minutes, and then cooled on ice. The samples were centrifuged by 14,500 rpm for 15 minutes, and then the supernatants were collected. The amounts of harvested protein were determined based on OD 595 using Bradford solution. Equal amounts of protein (30 μg each) underwent electrophoresis (200V, 45 minutes) on READYGELS J (7.5%; Bio-Rad, Tokyo, Japan). After semidry blotting was performed (242mA, 1 hour), the membrane was reacted with first (4°C, overnight) and horseradish peroxidase-conjugated second (room temperature, 1 hour) antibodies. The signals were analyzed using Lumi-Imager F1 (Roche Molecular Biochemicals, Tokyo, Japan).

FACS Analysis of Muscle Mononuclear Cells

The visible nerves, blood vessels, and tendons of the whole hind limb muscle of the denervated or intact side were removed with microsurgical forceps under a dissection microscope. Trimmed muscles were minced with scissors and then treated with 0.2% collagenase type 2 under stir for 40 minutes at 37°C. Digested muscles were filtered through a 100-μm and subsequently a 40-μm filter, and then red blood cells were removed by treatment with 0.8% NH_4Cl. The mononuclear cells obtained were suspended in 100 μl of PBS and reacted with antibodies. The first antibody (on ice, 30 minutes) was allophycocyanin-conjugated anti-CD45, phycoerythrin (PE)-conjugated anti-CD11b, or biotin-conjugated anti-CD44. The second reagent for the biotin-conjugated anti-CD44 antibody was PE-conjugated streptavidine (on ice, 15

minutes). Finally, the samples were washed with PBS, dissolved in 1 ml of PBS with 2% bovine serum albumin, and analyzed by FACS.

BrdU Staining

Mice at day 4 were injected intraperitoneally with 50 μg/g body weight of BrdU in 200 μl of PBS. Two hours after the injection,[15] the mice were sacrificed by cervical dislocation. Fixation of the muscle sample was the same as that for immunohistochemistry. Cryostat sections (5 μm thick) were stained with chicken anti-GFP antibody and subsequently fluorescein isothiocyanate-conjugated anti-chicken IgG antibody. Next, after fixation of GFP with 2% formaldehyde, DNA was denatured by 2 N HCl and neutralized by 0.1 mol/L sodium 4-borate (pH 8.5). Then, BrdU staining with anti-BrdU antibody and subsequently Alexa Fluor 568-conjugated goat anti-mouse IgG was performed. The sample was examined under a confocal laser microscope.

Apoptotic Cell Detection

Apoptotic cells were detected on cryostat sections using ApopTag^R Red *In Situ* Apoptosis Detecting kit (Chemicon International Inc.) according to manufacturer's instructions. Briefly, cyostat sections were prepared as described in immunohistochemistry section. Next, GFP staining and fixation was performed as described under BrdU Staining. After being postfixed and permeabilized with pre-cooled (−20°C) mixture of ethanol and acetic acid (2:1), the sections were reacted with digoxigenin-labeled nucleotides under the presence of terminal deoxynucleotidyl transferase. Then, the sections were reacted with rhodamine-conjugated sheep polyclonal anti-digoxigenin antibody. Nuclei were stained with TOTO-3. Sections were examined under a confocal laser microscope.

Reverse Transcriptase-Polymerase Chain Reaction (RT-PCR)

Three fractions of mononuclear cells, GFP positive, GFP negative/CD44 positive, and GFP negative/CD44 negative, from four day 28 mice were isolated by FACS and diluted in PBS. Total RNA from 1 × 10^4 cells of each population was isolated using RNeasy (Qiagen, Tokyo, Japan) according to the manufacturer's instructions and reverse transcribed using oligo dT primers with a total reaction volume of 30 μl. The reverse transcription program was 25°C for 10 minutes, 48°C for 30 minutes, and then 95°C for 5 minutes. Polymerase chain reaction was performed using 3 μl of each RT product (cDNA), with a total reaction volume of 20 μl. The PCR thermal cycle was 94°C for 3 minutes, then 40 cycles (or 30 cycles for transforming growth factor (TGF)-β1) of 94°C for 15 seconds, 60°C for 30 seconds, and 72°C for 30 seconds, and finally 72°C for 5 minutes.

The primers for PCR were type I collagen (413-bp product) sense (5′-GTGAACCTGGCAAACAAGGT-3′) and antisense (5′-CTGGAGACCAGAGAAGCCAC-3′), MMP-14 (308-bp product) sense (5′-ACAAAGATGCCCCCTCAACC-3′) and antisense (5′-GCTTCGTCAAACCAGTGC-3′), MMP-3 (391-bp product) sense (5′-TTCTCCAGGATCTCTGAAGGAGAGG-3′) and antisense (5′-ATTTGGTGGGTTACCACGAGGACATC-3′), tenascin-C (355-bp product) sense (5′-GCCTCAACAACTGCTACAATCGTG-3′) and antisense (5′-TCAGCCCCTGTGAACCCATC-3′), α-smooth muscle actin (α-SMA) (240-bp product) sense (5′-GAGAAGCCCAGCCAGTCG-3′) and antisense (5′-CTCTTGCTCTGGGCTTCA-3′), and TGF-β1 (431-bp product) sense (5′-CTAATGGTGGACCGCAACAAC-3′) and antisense (5′-CGGTTCATGTCATGGATGGTG-3′). These primers were obtained from Qiagen. Primers for β-actin (540-bp product) were sense (5′-GTGGGCCGCTCTAGGCACCAA-3′) and antisense (5′-CTCTTTGATGTCACGCACGATTTC-3′). As positive controls for these primers, RNA samples from 8-week-old mouse mammary gland were used for MMP-3 and from mouse embryo (day 13) were used for the rest.

Antibodies and Chemicals

Collagenase type 2 was from Worthington Biochemical Corp. (Lakewood, NJ). Allophycocyanin-conjugated rat anti-mouse CD45 antibody (clone 30-F11), rat anti-mouse CD31 antibody (clone MO76917), PE-conjugated rat anti-mouse CD11b antibody (clone M1/70), and mouse anti-BrdU antibody (clone MO76134) were from Becton Dickinson (San Diego, CA). Rat biotin-conjugated anti-mouse CD44 antibody (clone KM201) was from Southern Biotechnology Associates, Inc. (Birmingham, AL). Rat anti-mouse laminin-α2 antibody (clone 4H8-2) was from Alexis Corp. (San Diego, CA). Rabbit polyclonal anti-mouse type I collagen antibody (for immunohistochemistry) was from Biogenesis Inc. (Kingston, NH). Rat anti-mouse tenascin-C antibody (clone Mtn12)[16] was kindly provided by Prof. Ekblom (Department of Animal Physiology, Uppsala University, Uppsala, Sweden). Goat polyclonal anti-rat C/EBPα antibody, rabbit polyclonal anti-m-cadherin antibody, goat polyclonal anti-mouse collagen α2 type I antibody (for Western blotting analysis), and rabbit polyclonal anti-human TGF-β1 antibody were from Santa Cruz Biotechnology (Santa Cruz, CA). Rabbit polyclonal anti-human α-SMA antibody was from Lab Vision Corp. (Fremont, CA). Rat anti-mouse N-CAM (clone MAB310) and chicken polyclonal anti-GFP antibody and ApopTag Red *In Situ* Apoptosis Detection kit were from Chemicon International Inc. (Temecula, CA). Alexa Fluor 594-conjugated goat anti-rat IgG antibody, Alexa Fluor 568-conjugated goat anti-rabbit IgG antibody, Alexa Fluor 594-conjugated donkey anti-goat IgG antibody, Alexa Fluor 568-conjugated goat anti-mouse IgG antibody, Alexa Fluor 594-conjugated α-bungarotoxin, and TOTO-3 iodide (642/660) were from Molecular Probes (Eugene, OR). Fluorescein isothiocyanate-conjugated donkey polyclonal anti-

chicken IgG antibody was from Jackson Immuno Research Laboratories (West Grove, PA). Horseradish peroxidase-conjugated rabbit anti-goat IgG antibody was from Zymed Laboratories Inc. (San Francisco, CA). The RNeasy Micro kit was from Qiagen.

TaqManR Reverse Transcription Reagents were from Roche Molecular Systems, Inc. (Branchburg, NJ). The Mouse β-actin Control Amplimer set was from CLONTECH Laboratories, Inc. (Palo Alto, CA). ECL Western Blotting Detection Reagents were from Amersham Biosciences (Little Chalfont, Buckinghamshire, United Kingdom).

Statistical Analysis

Results were expressed as means ± SD. For comparison between any two groups, Welch's *t*-test was applied based on results of the data analysis by F-test. A *P* value of less than 0.01 was considered to indicate statistical significance.

Results

Establishment of GFP BM Chimeric Mice

Fifty-three mice received bone marrow transplantation. Of these, 45 mice were sacrificed and analyzed. The mean bone marrow chimerism at the time of sampling was 88.5 ± 7.9%. One mouse died of unknown cause 16 days after the bone marrow transplantation. Five mice were excluded from the study because of scar contraction of the hind limb due to irradiation. Two mice died of deep anesthesia.

Muscle Fiber Atrophy, Increased Interstitial Cells, and Fibrosis in Denervated Muscle

To verify the condition of denervation, the decrease of the diameter of gastrocnemius muscle fibers was examined by analyzing immunohistochemical images. On the denervated side (left), the diameter was significantly decreased 4 days after denervation (day 4; Figure 1). Denervation was also ascertained by observation of separate unconnected stumps of the cut sciatic nerve. On H&E stain, an increase in the number of interstitial mononuclear cells was observed from day 4. They accumulated in perisynaptic regions, as reported in the literature.[1,2]

From day 14, progressive fibrosis was detected by H&E staining. Fibrotic change was also examined by immunostaining for type I collagen (Figure 3, c and d). Fatty change was not observed in C57BL/6J mice, at least up to 4 months after the denervation (day 112). In contrast, the hind limb muscles of BALB/c mice showed fatty change from 1 month after denervation (day 28; data not shown). This difference in phenotypic expression may be interpreted as the influence of background strain.

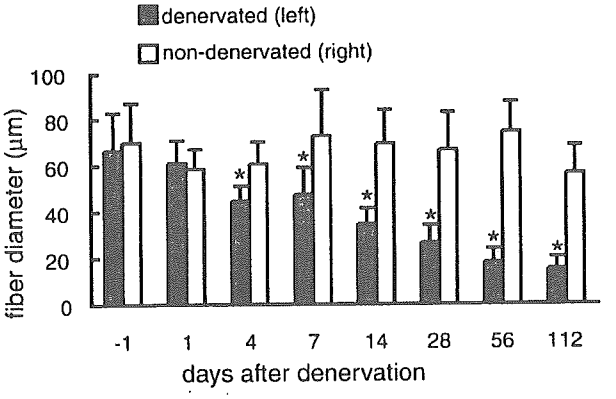

Figure 1. Decrease of muscle fiber diameter in denervated muscle. Diameters of muscle fibers of both denervated (**left, gray bar**) and nondenervated (**right, white bar**) gastrocnemius muscle were measured before denervation (−1) and 1 to 112 days after denervation. Bars represent the means ± SD of 50 fibers. $^*P < 0.01$.

BM-DCs Accumulated in the Perisynaptic Region

On day 4, many GFP-positive BM-DCs had entered the denervated (left) gastrocnemius muscle, mainly at the external fascia and perimysium (Figure 2, a and b). BM-DCs then faded out of these regions from day 7, but at the same time they appeared on the endomysium of each muscle fiber and gradually accumulated in the perisynaptic regions (Figure 3a). The time course of the appearance of BM-DCs in the perisynaptic region is shown in Figure 4, a and b. From day 4, BM-DCs significantly increased in the perisynaptic region to reach a maximum around days 14 to 28; thereafter, they gradually decreased. The initial accumulation at the perimysium on day 4 was excluded from this analysis. Distortions in the arrangements and decreases in the number of NMJs were also observed from 2 months after the denervation (day 56) and were more apparent on day 112 (Figure 3b).

When we compared the high-magnification fluorescent images of BM-DCs with that of H&E staining, BM-DCs accounted for considerable part of the interstitial mononuclear cells (Figure 2, c and d). Quantitative analysis showed that BM-DCs accounted for around 43% of the interstitial cells on day 4, 41% on day 14, and 39% on day 28, respectively (Figure 5a). However, as long as we considered only the shape of these increased interstitial cells, BM-DCs and muscle tissue-derived cells (MT-DCs) were indistinguishable under the microscope, and they were spindle or stellate shaped, as reported in the literature.[4]

BM-DCs Co-Localized with Expression of ECMs

Some fibrosis-related components of ECMs are known to accumulate around the perisynaptic regions of denervated skeletal muscle.[5] We examined whether BM-DCs co-localize with expressions of some components of ECMs. Type I collagen was detected in the perisynaptic regions in which BM-DCs were also accumulated (Figure 3, c and d). The accumulation of type I collagen was in

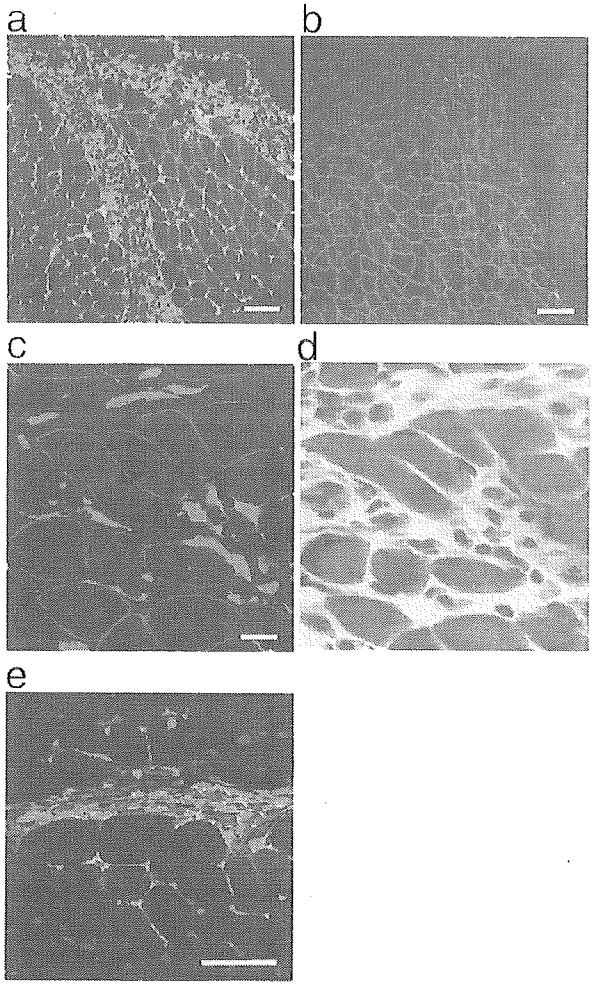

Figure 2. BM-DC infiltration into denervated muscle and co-localization with ECMs. Analysis by immunohistochemistry and H&E. **a:** Many BM-DCs (green; GFP) had infiltrated the external fascia and perimysium (green bands) and spread into the endomysium of denervated gastrocnemius muscle 4 days after denervation (day 4), whereas the nontreated side (**b**) showed no increase of BM-DCs (red; laminin-α2 representing basement membrane). Comparison at high magnification of GFP-positive cells (**c**; green) with interstitial mononuclear cells in H&E (**d**) shows that BM-DCs account for considerable part of the interstitial cells. **e:** Expression of tenascin-C (red) on day 4 at the perimysium, at which the BM-DC (green or merged with nucleus to light blue) accumulated. Within the perimysium, mononuclear MT-DCs (spindle-shaped areas with nuclei, lacking red signal) are also observed. TOTO-3 (dark blue) was used for nuclear staining. Scale bars = 100 μm (**a** and **b**), 20 μm (**c**), and 40 μm (**e**).

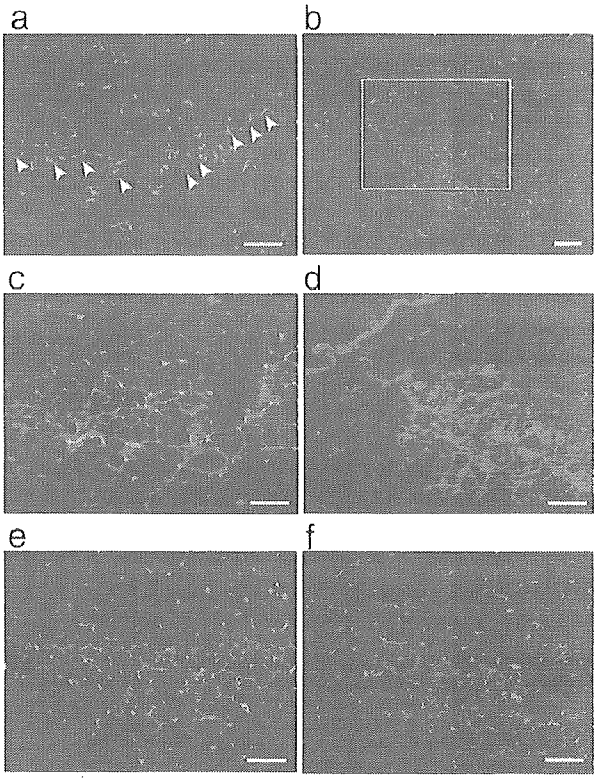

Figure 3. Accumulation of BM-DCs in the perisynaptic region and their co-localization with ECMs. Immunohistochemical analysis of day 28 (**a**, **c**, and **e**; serial sections) and day 112 (**b**, **d**, and **f**; serial sections). BM-DCs accumulated in the perisynaptic regions (**a** and **b**), co-localizing with type I collagen (**c** and **d**, red). BM-DCs also co-localized with tenascin-C on day 28 (**e**, red). Tenascin-C revealed spotted pattern on day 112, although still associating with BM-DCs (**f**, red). **Arrowheads** in **a** indicate individual NMJs (α-bungarotoxin, red). The box in **b** corresponds to the fields of **d** and **f**. Scale bars = 80 μm (**a** and **c** to **f**) and 100 μm (**b**).

accordance with the progressive fibrosis observed in H&E staining. However, immunoblotting analysis showed no evidence that total type I collagen protein had been increased in denervated entire gastrocnemius muscle compared with that of intact side (data not shown). Thus, even if there is increased synthesis of type I collagen in fibrotic lesion in denervated skeletal muscle, degradation of type I collagen may also be involved in the pathogenesis of fibrosis.[17]

The expression of tenascin-C, an anti-adhesion molecule, also accompanied the distribution of BM-DCs and appeared in the perisynaptic regions. On day 4, tenascin-C was detected around the invading BM-DCs or MT-DCs at the perimysium (Figure 2e). On day 7, tenascin-C disappeared from the perimysium, and BM-DCs also disappeared. After day 7, tenascin-C was again detected at the perisynaptic regions in which BM-DCs also accumulated (Figure 3e). This accumulation of tenascin-C might support the idea that tenascin-C appears at sites to which cells migrate, such as development, inflammation, tumorigenesis, and wound healing.[18] However, the expression pattern of tenascin-C was more distinctly restricted to each NMJ than that of type I collagen, especially on day 112 (Figure 3f). Thus, tenascin-C may initially regulate accumulation of BM-DCs at the perimysium, then in perisynaptic regions, and thereafter control, for example, the dynamic induction of regenerating axons to each NMJ. On the other hand, N-CAM[6] was uniformly distributed at each endomysium from day 4, showing no particular co-localization with BM-DCs (data not shown).

There is a possibility that BM-DCs can differentiate into particular cell lineages. Therefore, we examined several typical lineage markers. α-SMA is a marker for myofibroblasts or activated interstitial cells found in inflammatory or chronic lesions. The expression of α-SMA was not detected among BM-DCs and MT-DCs (data not shown). Whether BM-DCs incorporate into satellite cells in skeletal muscle is currently controversial.[19,20] In the present

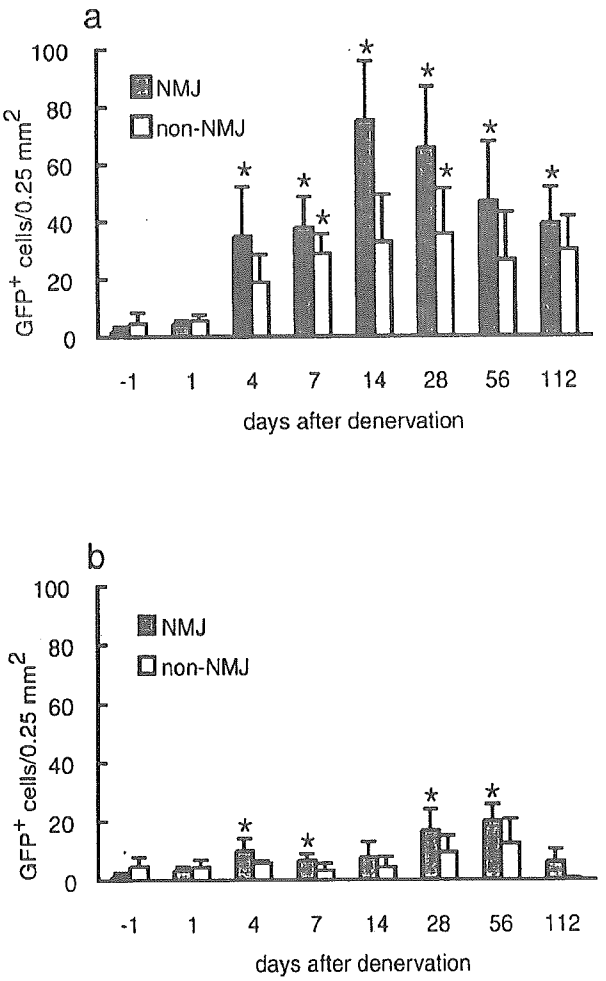

Figure 4. Increase of the BM-DCs in denervated gastrocnemius muscle. Time course of the BM-DC increase in left denervated (**a**) or right nontreated (**b**) side. Data are shown as numbers of GFP-positive cells per field (0.25 mm^2) including (**gray bars**) or excluding (**white bars**) NMJ regions. Bars represent the means ± SD of five fields. $^*P < 0.01$.

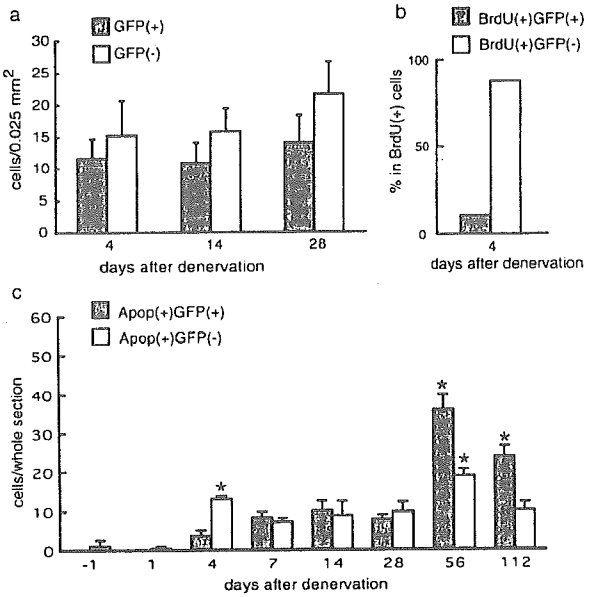

Figure 5. The ratio of BM-DCs among interstitial mononuclear cells in denervated gastrocnemius muscle and their proliferation or apoptotic activity. **a:** Numbers of BM-DCs (**gray bars**) and MT-DCs (**white bars**) around NMJs of denervated muscle. Data are shown as cell numbers per field (0.025 mm^2/field). Interstitial connective tissue was defined as tissue outside the muscle fiber basement membrane stained by laminin-α2. Mononuclear cells were defined by nuclear staining with TOTO-3. **b:** The proportion of interstitial cells (**gray bar**, GFP positive; **white bar**, GFP negative) that were BrdU positive after 2 hours of BrdU exposure in a whole cross-sectional area of gastrocnemius muscle 4 days after denervation. **c:** Time course of apoptotic activity of BM-DCs (**gray bars**) and MT-DCs (**white bars**) of denervated muscle. Data are shown as numbers of apoptotic (Apop) cells per whole muscle section. Bars represent the means ± SD of five fields (**a**) or three whole sections (**c**), respectively. $^*P < 0.01$.

study, GFP-positive satellite cell was not detected in denervated muscle. None of the other lineage markers tested, including CD31 (platelet/endothelium cell adhesion molecule-1) for vascular endothelium, neonatal myosin heavy chain for developing myofibers, and C/EBP-α for adipose cells, was detected among those interstitial cells. Thus, BM-DCs were revealed to be negative for some typical lineage markers, although sparing the possibility that they are fibroblasts.[21]

GFP-positive BM-DCs were also observed in gastrocnemius muscles of the intact side or bilateral nondenervated muscle (Figure 4, a and b). Inappropriate homing of hematopoietic or mesenchymal stem cells resulting from peripheral intravenous injection of bone marrow cells may have caused the survival of these cells. These cells may also reflect the existence of migrant, but long-term-resident, muscle interstitial cells. However, significant increase of BM-DCs in the intact side (Figure 4b) may due to sensitization via denervated leg.

BM-DCs in Denervated Skeletal Muscle Had Monocyte/Macrophage Phenotype

To investigate whether BM-DCs retain a hematopoietic lineage even in denervated skeletal muscle, we tested them for CD45 and CD11b by FACS analysis of total mononuclear cells harvested from whole denervated muscle and by immunohistochemistry of corresponding samples. On FACS analysis, at least up to day 28, the GFP-positive population was revealed to be CD45- and CD11b-positive (Figure 6, a and b). These results again showed that BM-DCs have not *trans*-differentiated into a nonhematopoietic lineage, including fibroblastic, angiogenic, myogenic, adipogenic, or neurogenic lineage, but are fundamentally of monocyte/macrophage lineage.

Next, we tried to define the migrating nature of the increased interstitial cells including BM-DCs and mononuclear MT-DCs by their CD44 expression. CD44 is an adhesive molecule known as an ECM (hyaluronan) receptor[22] that is broadly expressed on the surface of hematopoietic[23] and nonhematopoietic cells of vertebrates. CD44 is involved in lymphocyte homing, macrophage or lymphocyte activation, and tumor metastasis.[24–26] CD44 connects actin filaments with MMP-14 (membrane type 1-MMP; MT1-MMP), which is a representative of membrane type MMP,[27] or activates proMMP-2 at the forward processes (lamellipodia) of such migrating cells.[28] Put together, we expected the

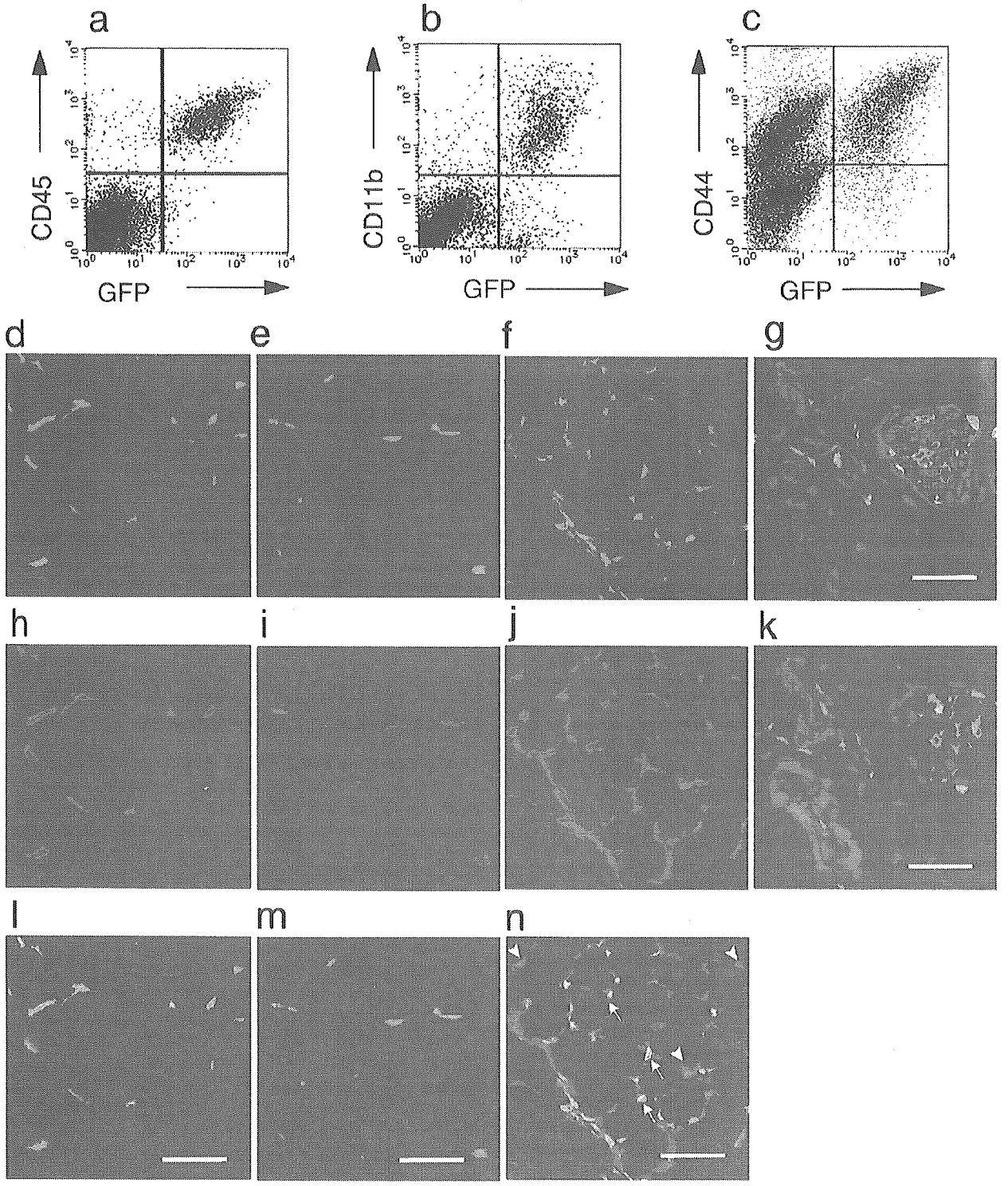

Figure 6. Flow cytometric and immunohistochemical analysis of increased mononuclear interstitial cells in denervated muscle. **a** to **c:** Mononuclear cells were isolated from gastrocnemius muscle 4, 14, and 28 days after the denervation. Following appropriate immunostaining, the cells were analyzed by flow cytometry. Representative results of analysis of isolated mononuclear cells 4 days after the denervation for GFP and CD45 (**a**), CD11b (**b**), and CD44 (**c**). **d** to **n:** Immunohistochemical analysis of BM-DCs in gastrocnemius muscle 14 days after the denervation. Almost all GFP-positive cells (**d** to **f**; green) co-stained with CD45 (**h**; red) and CD11b (**i**, red) and therefore revealed a merged expression pattern for these antigens (**l** and **m**; merged into yellow). On the other hand, CD44-positive cells (**j**; red) were GFP positive (**f**, **j**, and **n**; **arrows**) or GFP negative (**f**, **j**, and **n**; **arrowheads**). **g** and **k:** Serial sections of a neuro-vascular bundle in a gastrocnemius muscle 4 days after denervation stained for CD44 (**g**; red) or α-SMA (**k**;, red). TOTO-3 (blue) was used for nuclear staining. Scale bars = 40 μm.

increased mononuclear interstitial cells migrating to the perisynaptic regions to be CD44 positive whether they were BM-DCs or MT-DCs. Accordingly, CD44-positive mononuclear cells contained both GFP-positive and GFP-negative fractions (Figure 6c, top right and top left fractions, respectively). These fractions were supposed to reflect BM-DCs and mononuclear MT-DCs, respectively.

Immunohistochemical analysis supported those findings. Almost all BM-DCs were CD45 positive up to 2 months after the denervation (day 56; Figure 6, d, h, and l) and CD11b positive at least up to 4 months after the denervation (day 112) (Figure 6, e, i, and m, respectively). In addition, almost all interstitial mononuclear cells that might include BM-DCs and mononuclear MT-DCs were positive for CD44 at least up to day 112 (Figure 6, f, j, and n).

Observation of the posterior tibial artery revealed that vascular endothelial cells are CD44 negative (Figure 6, g and k). However, the tibial nerve trunk contained CD44-positive but GFP-negative cells, which were revealed to be Schwann cells by comparing them with a serial section stained with S-100 protein (Figure 6g; data not shown). Some of the large GFP-positive cells observed within the nerve trunk in Figure 6g may be macrophages that are involved in phagocytosis of degenerated axons.[15] Combining the mononuclear cell count with the fractional percentile of FACS-gated cells suggested that the denervated (left) gastrocnemius muscle contained around three to four times as many BM-DCs by muscle weight than the nondenervated (right) side (data not shown).

Poor Proliferation Activity of BM-DCs

There is a possibility that the GFP-positive cells observed in the denervated gastrocnemius muscle originated from muscle tissue-derived GFP-positive interstitial cells: long-term residents of skeletal muscle were found in the non-denervated side. In addition, the increase of the GFP-positive cells may depend on their proliferation by dividing or on a constant supply from the circulation system.

To answer these questions, we performed BrdU staining of denervated gastrocnemius muscle on day 4, the time point of the maximum reported proliferation activity of the increased interstitial cells.[2,3] GFP-positive interstitial cells formed only a very small minority of the BrdU-positive population in the denervated gastrocnemius muscle of day 4 (Figure 5b). Because GFP-positive cells accounted for nearly half of the increased interstitial cells in denervated gastrocnemius muscle on day 4 (Figure 5a), this result suggests poor proliferation potential of the GFP-positive population. Taking only the short life span of blood cells into consideration, it is further suggested that the majority of the increased GFP-positive cells in denervated muscle are not muscle tissue-derived dividing cells but are a bone marrow-derived and continuously supplied population.

Contribution of Apoptosis to the Decrease in Number of BM-DCs

The gradual decrease in number of BM-DCs in denervated gastrocnemius muscle observed from day 28 may be due to decreased circulating-in, increased re-circulating, or increased apoptotic activity of BM-DCs. To assess the contribution of apoptosis to the decrease in number of BM-DCs, we performed quantitative analysis of apoptotic cells in denervated gastrocnemius muscle. GFP-positive apoptotic cells significantly increased in number from day 56 ($P < 0.01$; Figure 5c). The result suggests that increased apoptotic activity of BM-DCs contributed to the gradual decrease in number of BM-DCs in denervated skeletal muscle. Although implication of the increased apoptotic activity of GFP-negative cells (MT-DCs) on day 4 (Figure 5c) is unclear, apoptotic activity of MT-DCs generally followed that of BM-DCs, indicating cooperative cellular rolls among these populations.

BM-DCs Expressed TGF-β1

To distinguish the functional roles of BM-DCs and MT-DCs, we studied the gene expression patterns of these populations by RT-PCR (Figure 7a). Denervated skeletal muscle of day 28 mice was chosen because many BM-DCs had accumulated in the perisynaptic region at the date. As controls, bilateral intact hind limb muscles of bone marrow chimeric mice were used instead of those of the contra-lateral side of the denervated limb to exclude the possibility of any compensative up- or down-regulation of the genes.

In denervated muscle, the CD44-positive MT-DCs, which may reflect muscle tissue-derived mononuclear cells and Schwann cells (as shown in Figure 6g), mainly expressed type I collagen and tenascin-C, suggesting that this population contains fibroblasts as the main effector of fibrosis (Figure 7a, lane 2). In contrast, BM-DCs did not express type I collagen or tenascin-C; instead, they dominantly expressed TGF-β1, a principal growth factor known to promote fibrosis in persistent inflammation or to induce the synthesis of tenascin-C *in vitro* (Figure 7a, lane 1).[29] Immunohistochemical analysis showed dominant production of TGF-β1 protein by a portion of BM-DCs (Figure 7, b to d). TGF-β1 expressions by the CD44-positive MT-DCs, which potentially include fibroblasts, were not observed by RT-PCR (Figure 7a, lane 2) or immunohistochemically. However, slight to moderate amplification of TGF-β1 was detected from MT-DCs when PCR was performed by 40 cycles, in accordance with the common establishment that virtually all fibroblasts express TGF-β1 (data not shown). Despite being considered to only reflect vascular endothelial cells as shown in Figure 6k and therefore to express no particular molecules studied here, the CD44-negative MT-DCs also expressed type I collagen and tenascin-C (Figure 7a, lane 3).

We examined whether MMP- 3 (stromelysin-1), one of the soluble MMPs known to breakdown the largest variety

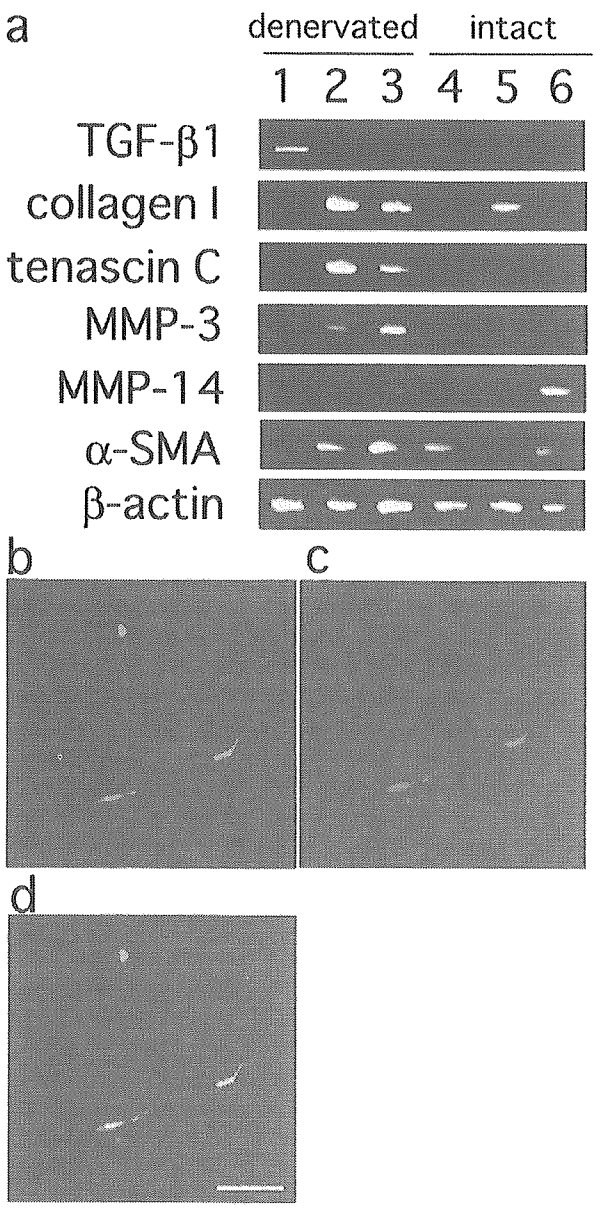

Figure 7. Expression patterns of fibrosis-related molecules within increased mononuclear interstitial cells in denervated muscle. **a:** RT-PCR analysis of fibrosis-related molecules of increased mononuclear interstitial cells in denervated muscle fractionated by FACS. Mononuclear interstitial cells were isolated from gastrocnemius muscle from either four mice 28 days after the denervation or intact mice. After appropriate immunostaining, approximately 1×10^4 cells in each fraction of GFP positive (**lanes 1** and **4**), GFP negative/CD44 positive (**lanes 2** and **5**), and GFP negative/CD44 negative (**lanes 3** and **6**) were collected by flow cytometry (corresponding to upper right, upper left, and lower left fractions in Figure 6c, respectively). After mRNA extraction from collected cells, RT-PCR was performed. Denervated mice (**lanes 1** to **3**), intact mice (**lanes 4** to **6**). **b** to **d:** Immunohistochemical detection of TGF-β1 protein in day 28 denervated gastrocnemius muscle. A portion of GFP-positive cells (**b**; green) co-stained with TGF-β1 at their cytoplasm (**c**; red) and therefore revealed a merged expression pattern (**d**; merged into yellow). Scale bars = 40 μm.

of substrates including gelatin, was expressed in the denervated muscle. MMP-3 is known to activate morphogenesis,[30] epithelial-to-mesenchymal conversion,[31] and carcinogenesis[32] of the mammary gland. MMP-3 was clearly detected in the denervated side especially in CD44-negative fraction (Figure 7a, lane 3). Although MMP-14 is reported to interact with CD44 on migrating cells,[27] less amplification of MMP-14 was detected in denervated muscle than in intact muscle. Further paradoxically, MMP-14 tended to be expressed in CD44-negative fraction (Figure 7a, lanes 3 and 6).

In MT-DCs of intact muscle, α-SMA was mainly expressed by CD44-negative fraction, probably reflecting vascular wall cells (Figure 7a, lane 6). In denervated muscle, both CD44-positive and -negative fractions showed up-regulation of α-SMA. This result may indicate an enhanced myofibroblastic phenotype in MT-DCs due to denervation, although α-SMA was not detected well among them immunohistochemically (Figure 7a, lanes 2 and 3). In denervated muscle, BM-DCs did not express α-SMA (Figure 7a, lane 1). Interestingly, BM-DCs did express α-SMA in intact muscle (Figure 7a, lane 4). Because BM cells were injected intravenously when establishing BM chimera, some of them, especially those that potentially express α-SMA, might have inappropriately homed into skeletal muscle. Therefore, such α-SMA-positive cells might, if small in number, occupy considerable proportion of BM-DCs in intact muscle, whereas α-SMA-negative migrant monocytes/macrophages might account for the majority of BM-DCs in denervated muscle. Thus, α-SMA may have been detected from BM-DCs in intact muscle and not in denervated muscle by analyzing the equal number of cells.

On the innervated side, very slight amplification of TGF-β1 expressed by BM-DCs was observed (Figure 7a, lane 4). Slight to moderate amplifications of type I collagen and tenascin-C were also observed in CD44-positive and -negative populations (Figure 7a, lanes 5 and 6). These signals may in general reflect the baseline or normal expressions of these genes.

Discussion

In this study, we proved that a great number of BM-DCs accounted for the increased number of interstitial cells in denervated skeletal muscle, in contrast to a previous study,[3] which concluded that the increased interstitial cells were derived from muscle tissue. In the experiment, white blood cell precursors were pre-labeled by repeated injection of titrated thymidine ([^{3}H]TdR) into subcutis of 7-to 10-week-old male albino mice 6 or 2 days before denervation. Determination of the presence of labeled leukocytes in denervated and control muscles was made 3 or 4 days after denervation by scintillation counting of muscle homogenates. As a consequence, incorporation of circulating-in cells into denervated extensor digitorum longus seemed unlikely in their study, although one of their time points of sampling was similar to one of those in our present study (day 4), on which an increased number of BM-DCs was observed. In contrast, bone marrow-chimeric animal enabled us to directly label bone marrow cells including mesenchymal stem cells and hematopoietic stem cells, to label peripheral leukocytes sufficiently, and to identify individual labeled cells. Thus, the negative result in the previous study for incorporation of BM-DCs

into denervated muscle may be due to technical limitations in labeling peripheral blood cells by radioisotopes or in detecting them.

Although the increased interstitial cells in denervated muscle have been currently identified as fibroblasts by electron microscopy, further intensive comparison of electron-microscopic images with that of the serial GFP fluorescent sections or immuno-electron microscopic study might enable observation of a distinction between BM-DCs and MT-DCs, bringing a novel morphological identification of these populations.

Evidence is emerging that BM-DCs play significant roles in fibrosis of other organs after progressive inflammation or injury. In pulmonary fibrosis, the majority of collagen-producing fibroblasts turned out to be bone marrow derived.[13,33] In renal fibrosis, about 14% to 15% of fibroblasts were bone marrow-derived,[12] in addition to the bone marrow monocytes that contribute to the growing process of fibrosis by facilitating the epithelial-mesenchymal transition.[34] In liver fibrosis, BM-DCs accounted for up to 22.2% of myofibroblasts: cells positive for α-SMA and vimentin and negative for CD45.[35]

In contrast, our results suggested that BM-DCs in denervated skeletal muscle were of a monocyte/macrophage lineage and therefore were not fibroblasts by definition of lineage-specific cell surface antigen, whereas that MT-DCs might contain fibroblasts. Thus, BM-DCs in denervated muscle were revealed not to differentiate into fibroblasts, as reported in fibrosis of some vital organs, but instead to maintain their monocyte/macrophage lineage. This inconsistency in the role of BM-DCs can be explained by the possibility that the pathology of denervated skeletal muscle is different from that of progressive inflammation in response to tissue injury. The increased interstitial cells in denervated muscle exhibited an anatomically characteristic distribution: they accumulated in perisynaptic regions of the denervated muscle. Interestingly, not only this accumulation but also the increase of interstitial cells itself is absent when the muscle is only immobilized by blocking the motor nerve with tetrodotoxin.[36] In addition, expression of tenascin-C or fibronectin is also undetected in such immobilized muscles.[36] These observations suggest that some signals related to denervation itself trigger the chemotaxis of macrophages to perisynaptic regions. These alterations may include axon degeneration, morphological alterations of Schwann cells around nerve terminals (terminal Schwann cells), and the lack of any substance usually supplied to the NMJ by axonal transport (Figure 8). One of the candidates for the signal factor may be monocyte chemoattractant protein-1 (MCP-1), a prototype of the CC chemokine. Mitigation of fibrosis by inhibiting monocyte infiltration with an MCP-1-blocking antibody or recently, by genetic intervention in the MCP-1 gene have been described in kidney,[37] lung,[38] and blood vessel.[39] Furthermore , MCP-1 is known to be produced by Schwann cells of denervated peripheral nerves and to induce infiltration by macrophages.[40] In denervated muscle, MCP-1 may be restrictedly expressed by terminal Schwann cells around

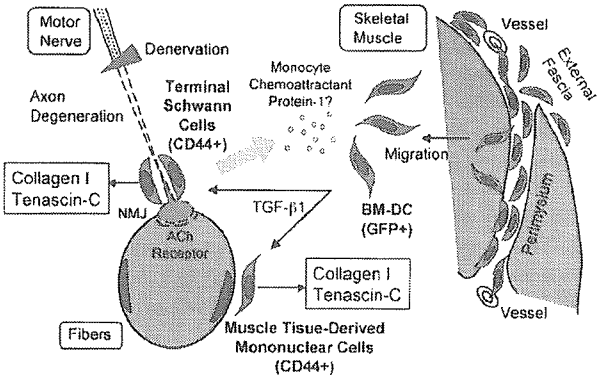

Figure 8. The cellular and molecular mechanisms of fibrosis in denervated skeletal muscle. Denervation-related signals (axon degeneration or cessation of axonal transport, for example) trigger release of chemokines such as MCP-1 from terminal Schwann cells. Circulating cells of macrophage/monocyte lineage originating from bone marrow (BM-DCs) are attracted by them and migrate to the perisynaptic region. The BM-DC release TGF-β1 to stimulate local (muscle tissue-derived) cells including fibroblasts or terminal Schwann cells to produce ECMs including type I collagen or tenascin-C. These ECMs might essentially support preservation of the position of each NMJ or induction of regenerating axons when reinnervated, although an excess of ECMs lead to fibrosis.

the perisynaptic region and may attract BM-DCs of macrophage/monocyte lineage (Figure 8).

We also showed for the first time the gene expression patterns of increased mononuclear interstitial cells in denervated skeletal muscle after dividing them into BM-DCs and MT-DCs by flow cytometric analysis. In contrast to fibrotic changes in some vital organs, BM-DCs never expressed components of ECMs, including type I collagen, in denervated muscle, whereas MT-DCs can be a main source of these ECMs. Instead, BM-DCs dominantly expressed TGF-β1, suggesting the regulatory role of BM-DCs in the fibrotic process (Figure 8). Although cultured fibroblasts isolated from denervated muscle were reported to express tenascin-C, those fibroblasts acquired the potential to produce it.[6] In addition, those "fibroblasts" might have contained other kinds of cells, including BM-DCs.

To determine functions of MT-DCs, we tried to clarify gene expression patterns of mononuclear interstitial cells by analyzing CD44-positive MT-DCs. Although all visible nerves and vessels, as shown in Figure 6, g and k, were removed before the samples were processed, immunohistochemical analysis suggested that the CD44-positive fraction possibly contained Schwann cells. One possible function of CD44 on Schwann cells is regulation of withdrawal of the myelin sheath from degenerated axons. The other possibility is that CD44 may support the connection of Schwann cells, especially perisynaptic ones (terminal Schwann cells), to muscle fibers at the position of the NMJ before denervation. This possibility may include the idea that Schwann cells also express type I collagen or tenascin-C themselves to hold their positions when denervated (Figure 8).

In the denervated side, not only the CD44-positive population but also the CD44-negative population expressed both type I collagen and tenascin-C, although these components of ECMs were more clearly detected in the CD44-positive population than in the CD44-nega-

tive population. Thus, the CD44-negative population may contain populations reactive to denervation. These may include muscle spindle cells, smooth muscle cells, vascular pericytes, perineural cells, and satellite cells. Some of these cells may express those components of ECMs or specifically express MMP-3 when denervated.

In conclusion, bone marrow-derived cells are suggested to regulate the pathogenetic process of fibrosis in denervated skeletal muscle. We believe that further investigation of the nature of BM-DCs will provide a novel approach that may lead to establishment of therapeutic amelioration of excessive fibrosis not only of denervated skeletal muscle but also of fatal neuromuscular disorders including amyotrophic lateral sclerosis as well as the latest investigations of fibrosis in other vital organs.

Acknowledgments

We are grateful to colleagues in our laboratory, in particular Dr. S. Fukada, for useful discussion and suggestions on this work.

References

1. McGeachie J, Allbrook D: Cell proliferation in skeletal muscle following denervation or tenotomy. Cell Tiss Res 1978, 193:259–267
2. Murray MA, Robbins N: Cell proliferation in denervated muscle: time course, distribution and relation to disuse. Neuroscience 1982, 7:1817–1822
3. Murray MA, Robbins N: Cell proliferation in denervated muscle: identify and origin of dividing cells. Neuroscience 1982, 7:1823–1833
4. Connor EA, McMahan UJ, Marshall RM: Cell accumulation in the junctional region of denervated muscle. J Cell Biol 1987, 104:109–120
5. Sanes JR, Schachner M, Covault J: Expression of several adhesive macromolecules (N-CAM, L1, tenascin (J1), NILE, uvomorulin, laminin, fibronectin, and a heparan sulfate proteoglycan) in embryonic, adult, and denervated adult skeletal muscle. J Cell Biol 1986, 102:420–431
6. Gatchalian CL, Schachner M, Sanes JR: Fibroblasts that proliferate near denervated synaptic sites in skeletal muscle synthesize the adhesive molecules tenascin (J1), N-CAM, fibronectin, and a heparan sulfate proteoglycan. J Cell Biol 1989, 108:1873–1890
7. Pereira RF, Halford KW, O'Hara MD, Leeper DB, Sokolov BP, Pollard MD, Bagasra O, Prockop DJ: Cultured adherent cells from marrow can serve as long-lasting precursor cells for bone, cartilage, and lung in irradiated mice. Proc Natl Acad Sci USA 1995, 92:4857–4861
8. Zhou S, Schuetz JD, Bunting KD, Colapietro AM, Sampath J, Morris JJ, Lagutina I, Grosveld GC, Osawa M, Nakauchi H, Sorrentino BP: The ABC transporter Bcrp1/ABCG2 is expressed in a wide variety of stem cells and is a molecular determinant of the side-population phenotype. Nat Med 2001, 7:1028–1034
9. Ferrari G, De Angelis GC, Coletta M, Paolucci E, Stornaiuolo A, Cossu G, Mavilio F: Muscle regeneration by bone marrow-derived myogenic progenitors. Science 1998, 279:1528–1530
10. Gussoni E, Soneoka Y, Strickland CD, Buzney EA, Khan MK, Flint AF, Kunkel LM, Mulligan RC: Dystrophin expression in the mdx mouse restored by stem cell transplantation. Nature 1999, 401:390–394
11. Sata M, Saiura A, Kunisato A, Tojo A, Okada S, Tokuhisa T, Hirai H, Makuuchi M, Hirata Y, Nagai R: Hematopoietic stem cells differentiate into vascular cells that participate in the pathogenesis of atherosclerosis. Nat Med 2002, 8:403–409
12. Iwano M, Plieth D, Danoff TM, Xue C, Okada H, Neilson EG: Evidence that fibroblasts derive from epithelium during tissue fibrosis. J Clin Invest 2002, 110:341–350
13. Hashimoto N, Jin H, Liu T, Chensue SW, Phan SH: Bone marrow-derived progenitor cells in pulmonary fibrosis. J Clin Invest 2004, 113:243–252
14. Okabe M, Ikawa M, Kominami K, Nakanishi T, Nishimune Y: 'Green mice' as a source of ubiquitous green cells. FEBS Lett 1997, 407:313–319
15. Mueller M, Leonhard C, Wacker K, Ringelstein EB, Okabe M, Hickey WF, Kiefer R: Macrophage response to peripheral nerve injury: the quantitative contribution of resident and hematogeneous macrophages. Lab Invest 2003, 83:175–185
16. Talts JF, Eng H, Zhang HY, Faissner A, Ekblom P: Characterization of monoclonal antibodies against tenascin-C: no apparent effect on kidney development in vitro. Int J Dev Biol 1997, 41:39–48
17. Savolainen J, Myllyla V, Myllyla R, Vihko V, Vaananen K, Takala TE: Effects of denervation and immobilization on collagen synthesis in rat skeletal muscle and tendon. Am J Physiol 1988, 254:R897–R902
18. Chiquet-Ehrismann R: Tenascins, a growing family of extracellular matrix proteins. Experientia 1995, 51:853–862
19. LaBarge MA, Blau HM: Biological progression from adult bone marrow to mononucleate muscle stem cell to multinucleate muscle fiber in response to injury. Cell 2002, 111:589–601
20. Ojima K, Uezumi A, Miyoshi H, Masuda S, Morita Y, Fukase A, Hattori A, Nakauchi H, Miyagoe-Suzuki Y, Takeda S: Mac-1^{low} early myeloid cells in the bone marrow-derived SP fraction migrate into injured skeletal muscle and participate in muscle regeneration. Biochem Biophys Res Commun 2004, 321:1050–1061
21. Strutz F, Okada H, Lo CW, Danoff T, Carone RL, Tomaszewski JE, Neilson EG: Identification and characterization of a fibroblast marker: FSP1. J Cell Biol 1995, 130:393–405
22. Aruffo A, Stamenkovic I, Melnick M, Underhill CB, Seed B: CD44 is the principal cell surface receptor for hyaluronate. Cell 1990, 61:1303–1313
23. Trowbridge IS, Lesley R, Schulte R, Hyman R, Trotter J: Biochemical characterization and cellular distribution of a polymorphic, murine cell-surface glycoprotein expressed on lymphoid tissues. Immunogenetics 1982, 15:299–312
24. Schmits R, Filmus J, Gerwin N, Senaldi G, Kiefer F, Kundig T, Wakeham A, Shahinian A, Catzavelos C, Rak J, Furlonger C, Zakarian A, Simard JJL, Ohashi PS, Paige CJ, Gutierrez-Ramos JC, Mak TW: CD44 regulates hematopoietic progenitor distribution, granuloma formation, and tumorigenicity. Blood 1997, 90:2217–2233
25. Protin U, Schweighoffer T, Jochum W, Hilberg F: CD44-deficient mice develop normally with changes in subpopulations and recirculation of lymphocyte subsets. J Immunol 1999, 163:4917–4923
26. Naot D, Sionov RV, Ish-Shalom D: CD44: structure, function, and association with the malignant process. Adv Cancer Res 1997, 71:241–319
27. Mori H, Tomari T, Koshikawa N, Kajita M, Itoh Y, Sato H, Tojo H, Yana I, Seiki M: CD44 directs membrane-type 1 matrix metalloproteinase to lamellipodia by associating with its hemopexin-like domain. EMBO J 2002, 21:3949–3959
28. Itoh Y, Takamura A, Ito N, Maru Y, Sato H, Suenaga N, Aoki T, Seiki M: Homophilic complex formation of MT1-MMP facilitates proMMP-2 activation on the cell surface and promotes tumor cell invasion. EMBO J 2001, 20:4782–4793
29. Pearson CA, Pearson D, Shibahara S, Hofsteenge J, Chiquet-Ehrismann R: Tenascin: cDNA cloning and induction by TGF-β. EMBO J 1988, 7:2977–2982
30. Wiseman BS, Sternlicht MD, Lund LR, Alexander CM, Mott J, Bissell MJ, Soloway P, Itohara S, Werb Z: Site-specific inductive and inhibitory activities of MMP-2 and MMP-3 orchestrate mammary gland branching morphogenesis. J Cell Biol 2003, 162:1123–1133
31. Lochter A, Galosy S, Muschler J, Freedman N, Werb Z, Bissell MJ: Matrix metalloproteinase stromelysin-1 triggers a cascade of molecular alterations that leads to stable epithelial-to-mesenchymal conversion and a premalignant phenotype in mammary epithelial cells. J Cell Biol 1997, 139:1861–1872
32. Sternlicht MD, Lochter A, Sympson CJ, Huey B, Rougier JP, Gray JW, Pinkel D, Bissell MJ, Werb Z: The stromal proteinase MMP3/stromelysin-1 promotes mammary carcinogenesis. Cell 1999, 98:137–146
33. Dunsmore SE, Shapiro SD: The bone marrow leaves its scar: new concepts in pulmonary fibrosis. J Clin Invest 2004, 113:180–182
34. Sato M, Muragaki Y, Saika S, Roberts AB, Ooshima A: Targeted disruption of TGF-β1/Smad3 signaling protects against renal tubulo-

interstitial fibrosis induced by unilateral ureteral obstruction. J Clin Invest 2003, 112:1486–1494
35. Forbes SJ, Russo FP, Rey V, Burra P, Rugge M, Wright NA, Alison MR: A significant proportion of myofibroblasts are of bone marrow origin in human liver fibrosis. Gastroenterology 2004, 126:955–963
36. Connor EA, Qin K, Yankelev H, DeStefano D: Synaptic activity and connective tissue remodeling in denervated frog muscle. J Cell Biol 1994, 127:1435–1445
37. Wada T, Furuichi K, Sakai N, Iwata Y, Kitagawa K, Ishida Y, Kondo T, Hashimoto H, Ishiwata Y, Mukaida N, Tomosugi N, Matsushima K, Egashira K, Yokoyama H: Gene therapy via blockade of monocyte chemoattractant protein-1 for renal fibrosis. J Am Soc Nephrol 2004, 15:940–948
38. Inoshima I, Kuwano K, Hamada N, Hagimoto N, Yoshimi M, Maeyama T, Takeshita A, Kitamoto S, Egashira K, Hara N: Anti-monocyte chemoattractant protein-1 gene therapy attenuates pulmonary fibrosis in mice. Am J Physiol Lung Cell Mol Physiol 2004, 286:L1038–L1044
39. Gosling J, Slaymaker S, Gu L, Tseng S, Zlot CH, Young SG, Rollins BJ, Charo IF: MCP-1 deficiency reduces susceptibility to atherosclerosis in mice that overexpress human apolipoprotein B. J Clin Invest 1999, 103:773–778
40. Tofaris GK, Patterson PH, Jessen KR, Mirsky R: Denervated Schwann cells attract macrophages by secretion of leukemia inhibitory factor (LIF) and monocyte chemoattractant protein-1 in a process regulated by interleukin-6 and LIF. J Neurosci 2002, 22:6696–6703

Human Molecular Genetics, 2005, Vol. 14, No. 6 *775–783*
doi:10.1093/hmg/ddi072
Advance Access published on February 2, 2005

ε-Sarcoglycan compensates for lack of α-sarcoglycan in a mouse model of limb-girdle muscular dystrophy

Michihiro Imamura[1,*], Yasushi Mochizuki[1,2], Eva Engvall[3] and Shin'ichi Takeda[1]

[1]Department of Molecular Therapy, National Institute of Neuroscience, NCNP, 4-1-1 Ogawahigashi-cho, Kodaira, Tokyo 187-8502, Japan, [2]Department of Plastic and Reconstructive Surgery, Graduate School of Medicine, University of Tokyo, Bunkyo-ku, Tokyo 113-0033, Japan and [3]The Burnham Institute, La Jolla, CA 92037, USA

Received October 18, 2004; Revised and Accepted January 24, 2005

Dystrophin and the dystrophin-associated protein (DAP) complex protect the sarcolemma against contraction-induced injury and serve as a mechanical link between the extracellular matrix and the actin cytoskeleton. Some of the functional properties of the DAP complex are mediated by its sarcoglycan (SG) subcomplex, which is composed of α-, β-, γ- and δ-SGs. Autosomal recessive limb-girdle muscular dystrophy type-2D (LGMD 2D) results from reduction in SG subcomplex levels caused by specific mutations in the muscle-specific *α-SG* gene. ε-SG is a widely expressed homolog of the muscle-specific α-SG, and expression of ε-SG may compensate for the pathologic changes in α-SG function. Thus, the goal of the present study was to investigate whether overexpression of ε-SG can compensate for dysfunction of α-SG. Several transgenic mouse lines that overexpress ε-SG in skeletal muscle were established. Overexpression of ε-SG in normal mice resulted in substitution of ε-SG for α-SG in the SG complex of skeletal muscle without any obvious abnormalities. To determine whether an increase in ε-SG expression may prevent muscular dystrophy in the context of α-SG-deficiency, these ε-SG transgenic mice were crossed with α-SG deficient mice. α-SG-deficient mice overexpressing ε-SG exhibited no skeletal muscle cell membrane damage or abnormal contraction. These data suggest that the overexpression of ε-SG may represent a therapeutic strategy for treatment of LGMD 2D.

INTRODUCTION

Sarcoglycans (SGs) are essential constituents of the dystrophin-associated protein (DAP) complex, which consists of several membrane-spanning and cytoplasmic proteins, including dystroglycans (α and β), SGs (α, β, γ and δ), sarcospan, syntrophins (α1, β1 and β2) and dystrobrevins that directly or indirectly associate with dystrophin (1–3). Dystrophin is an actin-binding cytoskeletal protein that mediates the association of cytoplasmic microfilaments to dystroglycan, which binds to laminin in the extracellular matrix (4). The dystrophin–DAP complex functions to protect the plasma membrane of striated muscle fibers from contraction-induced mechanical stress (3,5).

α-, β-, γ- and δ-SGs are membrane-spanning glycoproteins that associate with α- and β-dystroglycan and sarcospan (6,7). A defect in any one of the four SGs can disrupt the entire SG complex and lead to limb-girdle muscular dystrophy (LGMD types 2C–2F) (8–13). Analyses of striated muscle of SG-deficient animals have shown that the loss of the SG complex destabilizes interactions between α- and β-dystroglycans and between dystrophin and β-dystroglycan (14–16). These findings indicate that SGs play an important role in stabilizing the molecular axis of the dystrophin–DAP complex, but are functional only when they exist as a complex.

α-SG deficiency causes muscular dystrophy in human (LGMD 2D). α-SG and ε-SG appear closely related to each other at the amino acid sequence level; however, their tissue and cell localization differs (17,18). Whereas α-SG is only expressed in striated muscle, ε-SG is expressed in a variety of tissues including striated muscle, smooth muscle, lung, liver, kidney, spleen, testis, sciatic nerve and brain (17,19,20). Loss-of-function mutations in the *ε-SG* gene (*SGCE*) cause myoclonus–dystonia syndrome rather than muscular dystrophy (21). α-SG deficiency causes a significant

*To whom correspondence should be addressed. Tel: +81 423461720; Fax: +81 423461750; Email: imamura@ncnp.go.jp

reduction in formation of the SG subcomplex in the dystrophin–DAP complex, but residual SG complexes may form in the absence of α-SG and are composed of ε-, β-, γ- and δ-SGs (22). In fact, an ε-SG complex represents a major SG complex in certain cells including smooth muscle cells (23,24). However, although ε-SG may be functionally similar to α-SG, the low level of residual ε-SG complex in skeletal muscle cells does not prevent the development of muscular dystrophy in α-SG-deficient mice (22,25). Therefore, the goal of the present study was to determine whether overexpression of ε-SG may compensate for α-SG deficiency and prevent the muscular dystrophy phenotype in α-SG-deficient mice.

To investigate whether an increase in levels of the minor SG complex in skeletal muscle prevents muscular dystrophy in α-SG-deficiency, transgenic mice overexpressing mouse ε-SG were generated. In a wild-type background, overexpression of ε-SG reduced the amount of α-SG at the sarcolemma and increased the incorporation of ε-SG into an SG complex without obvious side effects. In an α-SG-deficient background, the increased ε-SG levels prevented the development of muscular dystrophy in mice up to at least 1 year of age. Biochemical and immunohistochemical analyses revealed that ε-SG overexpression resulted in the construction of a stable ε-SG-containing complex in the absence of α-SG.

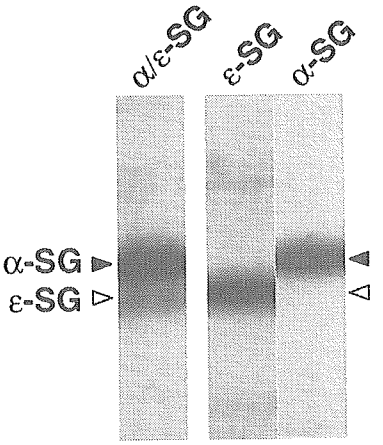

Figure 1. Expression of ε-SG protein in mouse skeletal muscle. Relative amounts of ε-SG and α-SG in mouse skeletal muscle were examined by immunoblotting using an antibody that recognizes a common region in α- and ε-SG (α/ε-SG). Immunoblotting with the α/ε-SG antibody detected two protein bands (50 and 46 kDa) in the skeletal muscle lysate of the C57BL/6 (B6) mouse, whereas the affinity-purified antibodies specific for α-SG (16) and ε-SG (19) detected only the 50 (solid arrowhead) and 46 KDa band (open arrowhead), respectively. The amount of ε-SG in muscle tissue was estimated as ~10% of that of α-SG.

RESULTS

Overexpression of ε-SG increases α-SG-deficient complex formation

Two types of SG complexes exist in normal skeletal muscle: a major complex, composed of α-, β-, γ- and δ-SGs, and a minor complex, composed of ε-, β-, γ- and δ-SGs (22). The minor complex exists even in α-SG deficiency, but it does not prevent the development of muscular dystrophy. Analysis demonstrated that the minor ε-SG-containing complex (ε–β–γ–δ) was present at levels that were less than one-tenth those of the major α-SG-containing complex in skeletal muscle (Fig. 1). To determine whether higher levels of the ε-SG complex can compensate for α-SG deficiency, transgenic mouse lines expressing ε-SG under muscle-specific γ-*SG* gene promoter were generated (Fig. 2A). The transgene product was tagged at the C-terminal with a c-myc sequence to distinguish it from endogenous ε-SG. Four independent mouse lines, e3, e17, e27 and e29 showed varying levels of ε-SG mRNA in the skeletal muscle (Fig. 2B). The ε-SG mRNA levels were the highest in the e17 line (30-fold of normal endogenous levels) and were the lowest in the e27 line (6-fold). Transgene expression appeared to correlate with slightly reduced levels of δ-SG, but did not affect the levels of the other SGs (α, β and γ). Interestingly, immunoblot analysis showed that the amount of ε-SG immunoreactivity, as a measure of protein level, did not correlate with ε-SG mRNA levels in the transgenic lines (Fig. 2C); all lines showed similar increases in ε-SG immunoreactivity levels in skeletal muscle, as compared to wild-type C57BL/6 (B6) mice. In contrast, the amount of α-SG immunoreactivity was markedly lower in all transgenic lines when compared with wild-type mice. Levels of other interaction partners of ε-SG (e.g. β- and δ-SGs and β-dystroglycan) were similar in skeletal muscle from transgenic and wild-type mice.

The 5′-gsg (mouse γ-*SG*) promoter/enhancer is less active in heart and testis than in skeletal muscle (26). Accordingly, c-myc-tagged ε-SG protein was only weakly detected in heart and absent in testis of e17 transgenic mice. Expression of the transgene had a minimal effect on α-SG protein levels in the heart (Fig. 2D).

Immunostaining of sections of quadriceps muscles from e17 mice using anti-SG antibodies demonstrated a marked increase in ε-SG-staining and a marked decrease in α-SG-staining of the sarcolemma (Fig. 3A), which is consistent with the immunoblotting results (Fig. 2C). However, the amounts and localizations of other SGs (β, γ and δ), sarcospan, dystrophin and utrophin remained unchanged. Similar results were obtained when using skeletal muscles from the three other transgenic lines, e3, e27 and e29 (data not shown). These finding suggest that overexpression of ε-SG replaced α-SG at the sarcolemma, and that the amount of ε-SG at the sarcolemma is limited by levels of other SGs, even when ε-SG is overexpressed.

Immunofluorescent staining of hearts from the e17 line revealed a mosaic pattern of transgene expression in a limited region of the ventricle (Fig. 3B). Relatively few cardiomyocytes showed high levels of c-myc-tagged ε-SG with low levels of α-SG expression. Most of the cardiomyocytes exhibited strong expression of α-SG at the cell membrane, which is consistent with the immunoblotting results (Fig. 2D).

To determine whether ε-SG replaced α-SG within the SG complex, interaction partners of ε-SG were immunoprecipitated from the leg muscle of transgenic mice (Fig. 3C). The anti-c-myc antibody co-immunoprecipitated ε-, β,- γ- and δ-SG as well as sarcospan and β-dystroglycan. The same pattern of co-precipitation was observed when an anti-β-SG